Section 10d: Surface-Specific Methods

UNIT 10d.1 Surface X-Ray Diffraction

INTRODUCTION

Surface X-ray Diffraction

Surface x-ray diffraction allows the determination of atomic structures of ordered crystal surfaces in an analogous way to x-ray crystallography for the determination of three-dimensional crystal structures. In doing this, crystallographic parameters such as lattice constants and Debye-Waller factors (thermal vibration amplitudes) are also accessed, so surface x-ray diffraction should be considered as a valid method for measuring these quantities too. Surface x-ray diffraction also probes surface morphological properties, such as roughness and facet formation, and allows the investigation of their thermodynamic and kinetic aspects, such as the study of phase transitions in surfaces.

Because x rays probe deep inside matter, buried interfaces can be treated in exactly the same manner as surfaces, so throughout this unit the words *surface* and *interface* will be used synonymously. In fact, some of the best applications of the method are for buried interfaces, where complementary electron-based probes such as low-energy electron diffraction (LEED; *UNIT 11c.1*) and reflection high-energy electron diffraction cannot reach.

Surface x-ray diffraction is not a laboratory technique. While there are one or two exceptions of installations in individual laboratories, the majority are associated with national or international facilities. Even the very early experiments carried out by Eisenberger and Marra (1981) used synchrotron radiation. By now, facility-based science is already rather common and will become more so in the future, as it has considerable economies of scale and advantages of centralized operational safety. The practice of surface x-ray diffraction should necessarily be considered as a facility-based operation, and it will be assumed that the reader will have access as a "user" to one of these facilities. This is usually handled by the submission of a proposal to be judged on the importance of the science to be carried out. Access is then usually free of charge.

Because surface x-ray diffraction is facility based, it is not a technique for which one can purchase the equipment piecemeal from a vendor. Every surface x-ray diffraction installation is slightly different, but most were derived from and are based on the description that follows, which is the X16A facility of the National Synchrotron Light Source (NSLS). Others, such as the Advanced Photon Source (APS, Argonne), the European Synchrotron Radiation Facility (ESRF, Grenoble), Hamburger Synchrotronstrahlungslabor (HASYLAB, Hamburg), Daresbury Laboratory, Photon Factory (PF, Tsukuba), and Laboratoire pour l'Utilisation de Rayonnement Synchrotron (LURE, Orsay), use basically the same control and analysis programs and procedures as those described here.

Competitive and Related Techniques

The need to travel to a facility to make surface x-ray diffraction measurements can be inconvenient, to say the least, so it is important to discuss its strengths and weaknesses compared with other techniques. Scanning probe methods, such as scanning tunneling microscopy (STM, *UNIT 11b.1*) and atomic force microscopy (AFM), are extensively used in surface science. These imaging methods are unbeatable for detecting singular events on surfaces, and the "microscopist's eye" will often detect a wide variety of local behavior. Thus STM has been very important in understanding instabilities of surfaces, step properties, and island morphologies during growth. When "average" quantities are needed for understanding general behavior, such as thermodynamics, the averaging must be carried out explicitly; diffraction methods will access ensemble-average quantities directly and will filter out the exceptions. This is particularly important when studying the dynamical behavior associated with phase transitions, where the correlations within a moving arrangement of atoms can still be detected by diffraction. At their limit, scanning probe microscopies can reach atomic resolution, but they always detect the outermost features on a surface and will not see below the surface. Diffraction methods can attain atomic positions to an accuracy of 0.01 Å routinely, while scanning microscopies can only achieve that in the surface-normal direction under certain circumstances.

The direct competitors with surface x-ray diffraction are thus the various forms of electron diffraction (Chapter 11), which provide information of an analogous form: LEED, reflection high-energy electron diffraction (RHEED), and transmission electron diffraction (TED). Since electrons interact more strongly with matter than do x rays, there are some important differences. First, electron diffraction is dynamical and requires a nonlinear theory to explain the intensity of the diffraction seen. This has been accomplished by deriving a careful theoretical description of the electron as it interacts with the sample in the case of LEED and to a lesser extent for RHEED. After 20 years of development, the method has reached the

Contributed by I.K. Robinson
Methods in Materials Research (2000) 10d.1.1-10d.1.22

point where structures can be refined as well as just calculated, and thermal vibrations can now be included. With x rays, the simpler kinematical description can be used, which makes the calculations very easy, so that powerful refinement procedures can be followed. Transmission electron diffraction is near to this kinematical limit also, and the linear approximation has been successfully used to obtain surface structures. The potential user can make a choice between a hard experiment and an easy analysis in the case of x rays or between an easy experiment and a hard analysis in the case of electron diffraction.

Second, for the same reason, the penetration of x rays is significantly larger than electrons. The sensitivity of LEED and RHEED is limited to about four atomic layers, and the accuracy becomes reduced in the lower layers. To examine interfaces, LEED has been used, but it requires physical removal of half of the sample. X-rays are not limited in this way and have many applications for interfaces: an important example is the electrochemical interface, which can be studied in situ. Transmission electron diffraction falls in between: samples must be thinned to 100 to 1000 Å but can still contain interfaces. The small differences in accuracy that can be obtained in surface structure determination by the different diffraction techniques can be attributed to the accessible range of reciprocal space. X-ray diffraction and TED tend to have higher accuracy parallel to the surface, because the largest component of momentum transfer is usually in that direction. Low-energy electron diffraction is a backscattering technique, which tends to give more accurate coordinates in the normal direction.

It used to be said that the momentum resolution of x rays was an unmatchable asset, but this has become less important in recent years. First, the spot profile analysis LEED (SPA-LEED) method was developed by Sheithauer et al. (1986) as well as the spot profile analysis RHEED (SPA-RHEED) method by Müller and Henzler (1995). These offer momentum resolution, which is comparable to x-ray diffraction, and are commercially available from Omicron. Surface-phase transitions can now be studied as well with LEED or RHEED as with x-ray diffraction. Second, the merit of probing correlations extending over large distances in real space has diminished with the widespread availability of STM and AFM, which routinely scan the same range.

PRINCIPLES OF THE METHOD

Surface is a generic word that is often used as an antonym to bulk. Deviations from physical properties of bulk matter are often attributed to (i.e., blamed on) "surface effects." The study of surfaces is therefore a productive way of understanding these deviations. The study of surfaces always starts with their structure, and that is what is probed with surface x-ray diffraction. Typical examples of surfaces, generalized to include internal interfaces, are shown in Figure 10d.1.1.

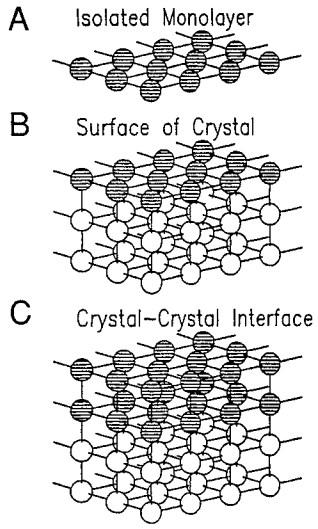

Figure 10d.1.1 Entities that can be studied with surface x-ray diffraction. (**A**) isolated monolayer (2D crystal). (**B**) Same as A but connected to a crystalline substrate. (**C**) Same as A but at the interface between two different crystals. From Robinson and Tweet (1992).

The general subject of diffraction will not be reviewed here since it appears elsewhere in this volume and also is covered in several excellent textbooks (James, 1950; Warren, 1969; Guinier, 1963; Lipson and Cochran, 1966; Woolfson, 1997). It is assumed that the reader is comfortable with the construction of a three-dimensional (3D) reciprocal space and the idea that the diffraction from a crystal is localized to a set of specific "Bragg" points forming a reciprocal lattice. Reciprocal space is spanned by the vectorial quantity **q**, which is the momentum transfer of the diffraction experiment. The axes of reciprocal space are chosen to lie along simple directions within the reciprocal lattice. The coordinates are then normalized so that the Bragg points appear at simple integers, called Miller indices, *hkl*. This construction of reciprocal space was introduced in *UNIT 1d.1* and will be assumed henceforth.

In surface x-ray diffraction, it is conventional to choose a coordinate system in reciprocal space that places the third index of the momentum transfer, q_z, perpendicular to the surface. This is usually compatible with the Miller index notation because the naturally occurring surfaces are usually close-packed planes of atoms, which have small-integer Miller indices according to the usual construction. This convention often requires use of an unusual setting of the bulk crystal unit cell, e.g., hexagonal for a cubic (111) surface or tetragonal for a cubic (110) surface. The convention is exactly the same as that used in LEED; see *UNIT 11c.1*. Another common terminology is to separate the components of momentum transfer, **q**, parallel and perpendicular to the surface by writing $\mathbf{q} = (q_P, q_z)$. Here q_P strictly represents *both* in-plane components. The reason for this separation is that a surface is a highly anisotropic object with completely different properties in the two directions.

Diffraction from Surfaces

The most important characteristic of diffraction from surfaces is illustrated as a 3D sketch in Figure 10d.1.2, which corresponds roughly to Figure 10d.1.1 transformed into reciprocal space. Bulk crystal diffraction is concentrated at points of reciprocal space because of the 3D periodicity of the crystal. A surface or interface has reduced dimensionality, so its diffraction is no longer confined to a point but extends continuously in the direction perpendicular to the plane of the surface or interface. These lines of diffraction, sharp in two in-plane directions and diffuse in the perpendicular direction, are called rods. The diffraction pattern of a two-dimensional (2D) crystal, as illustrated in Figure 10d.1.2, is a 2D lattice of rods in reciprocal space.

A surface rarely exists as an isolated entity (Fig. 10d.1.1A) but is normally intimately connected to a substrate of bulk crystalline material (Fig. 10d.1.1B) or materials (Fig. 10d.1.1C). The diffraction is then a superposition of 3D and 2D features, points and rods, as shown. However, the periodicities of the two lattices are the same (by construction), and so their diffraction patterns will be intimately related. This causes the lateral positions of the features to align so that the intensity distributions merge together. The 2D rods line up between the 3D points, and the two features simply merge together. The resulting object in reciprocal space, illustrated in the bottom panel of Figure 10d.1.2, is called a crystal truncation rod (CTR). An example of an experimental study of a CTR is given below (see Practical Aspects of the Method).

Crystal truncation rods have been treated theoretically as extensions of bulk diffraction by Andrews and Cowley (1985), Afanas'ev and Melkonyan (1983), and Robinson (1986), and their connection to the surface structure has been derived. The sensitivity to the surface is found to vary smoothly along the rod. Near the divergence of the intensity at the 3D Bragg points, the intensity of the CTR depends only on the bulk structure, through its bulk structure factor. According to the kinematic theory of diffraction, the intensity follows a $(q_z - G_z)^{-2}$ law near each bulk Bragg peak at position $\mathbf{G} = (G_P, G_z)$. In the more precise dynamical theory discussed by Afanas'ev and Melkonyan (1983), this nonphysical divergence at $q_z = G_z$ becomes finite and follows a Darwin curve instead, but the asymptotic behavior remains the same as in the kinematic theory.

The connection between the intensity distribution along a CTR and the corresponding surface structure is illustrated by a simple calculation in Figure 10d.1.3. The full curve is for an ideally terminated simple-cubic lattice of atoms; its functional form is just $1/(\sin q_z)^2$, whose divergence at Bragg points $q = 2n\pi$ is clearly visible. The dashed curve corresponds to an outward displacement of a single layer of atoms at the surface; the intensity curve near the Bragg peaks, where there is little surface sensitivity, is barely changed, but the intensity at the CTR minimum is strongly modified. Finally, the dotted curve is for a rough surface, modeled by random omission of a fraction of the atoms in the top layer; here, again, the biggest effect is at the CTR minimum, this time with a symmetric drop of the intensity curve.

A simple rule of thumb is that the measurement is the most surface sensitive at the position on the CTR that is furthest from the bulk Bragg peaks, where the intensity is also weakest. This rule applies not only to the structure itself but also to the sensitivity to fluctuations in the surface, e.g., its roughness. In performing an experiment, one is frequently faced with a choice between surface sensitivity and

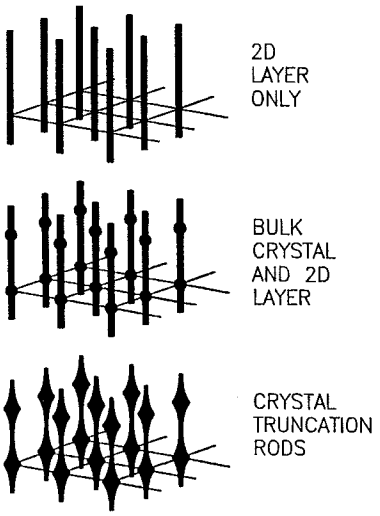

Figure 10d.1.2 Schematic of the diffraction from the objects in Figure 10d.1.1. The 3D points of reciprocal space are indicated as circles; 2D rods of reciprocal space are indicated as bars. From Robinson and Tweet (1992).

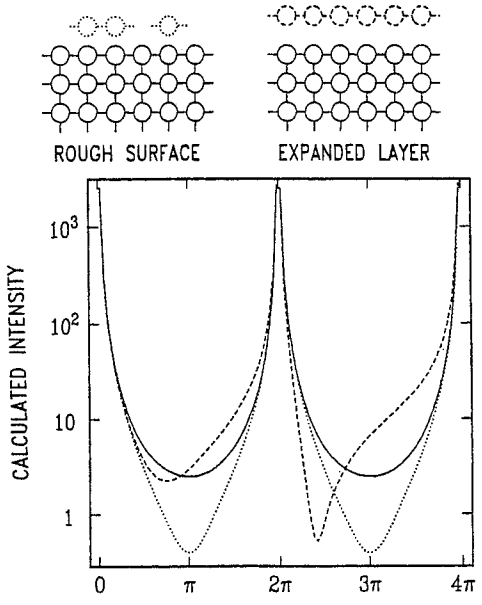

Figure 10d.1.3 Calculated CTRs for an ideally terminated surface (solid curve), a surface with modified top-layer spacing (dashed), and a rough surface (dotted). The intensity is plotted as a function of perpendicular momentum transfer, q_z, in normalized units.

signal level, since one quantity trades off directly with the other.

Measurement of Surface X-ray Diffraction

The surface x-ray diffraction signal can be measured with a standard diffractometer. For reasons explained below (see Practical Aspects of the Method), it is common to use a diffractometer with extra degrees of freedom. Synchrotron radiation is highly desirable as it results in convenient signal levels around hundreds to thousands of counts per second. The primary responsibility of the diffractometer is to select **q** by suitable choice of its angles while keeping the beam always on the center of the sample. Measurements then consist of scans of the **q** vector through the various features of the surface x-ray diffraction.

The shape and size of the resulting scans depend on the nature of the diffraction features being measured, e.g., due to the degree of order in the surface. The results also depend on the resolution function of the instrument, which is always convolved with the true diffraction pattern. The resolution function is controllable to a certain extent by instrumental parameters, particularly slits that define the beam divergence in different directions. The usual construction is shown in Figure 10d.1.4, which is based on the vector construction of **q** in terms of the incident and exit wave vectors $\mathbf{k}_i$ and $\mathbf{k}_f$: $\mathbf{q} = \mathbf{k}_i - \mathbf{k}_f$. The variation of $\mathbf{k}_i$ is represented by the angular width of directions allowed by the entrance slits and monochromator, $\Delta\alpha_M$, while the variation of $\mathbf{k}_f$ is defined by $\Delta\alpha_A$. The resulting resolution function is the shaded parallelogram at the top of the picture. Simple geometry shows that its dimensions parallel and perpendicular to the vector **q** are given by Moncton and Brown (1983):

$$\Delta q_{\parallel} = k(\Delta\alpha_M + \Delta\alpha_A)\cos\theta$$

$$\Delta q_T = k(\Delta\alpha_M + \Delta\alpha_A)\sin\theta \qquad (1)$$

where $k = 2\pi/\lambda$ is the length of both wave vectors and θ is half the diffraction angle 2θ.

Note that this picture applies to the scattering plane of the diffractometer, spanned by the 2θ angle of the diffractometer, and the notations Δq_P and Δq_T refer to parallel with (or radial) and transverse to the direction of **q**. The scattering plane is not the same as the surface plane of the sample, except in the grazing incidence geometry defined below, which is often used for precisely that reason. The third dimension of the resolution function, denoted $\Delta q_\perp$, is also defined by slits, this time in the direction perpendicular to the scattering plane; the resolution function then becomes a parallelogram-based prism by simple extension of Figure 10d.1.4 to 3D. This out-of-plane resolution is often the largest of the three because, in the grazing incidence geometry, the diffraction features are extended rods in that direction, and a considerable enhancement of intensity is thereby attained.

Many setups, including the one at X16A, gain additional flexibility by dividing the $\Delta q_\perp$ range into narrower sections by use of a linear position-sensitive detector (PSD). The x-ray counts recorded by the PSD are assigned a "position" along the detector by the height of its output pulse. This is accumulated in a multichannel analyzer (MCA) and then read out in bins, each corresponding to a section of $\Delta q_\perp$. The total counts in each bin are saved in the output file, to allow the data to be subsequently broken down into different q_z positions with a correspondingly narrower $\Delta q_\perp$. Since surface x-ray diffraction in the grazing incidence geometry should give features that are broad in q_z, all the bins should rise and fall together in intensity and give independent structure factors at different q_z values. However, if a powder grain or multiple scattering glitch happens to accidently satisfy the diffraction condition during some surface measurement, it will be recorded in only one MCA bin and can be suppressed.

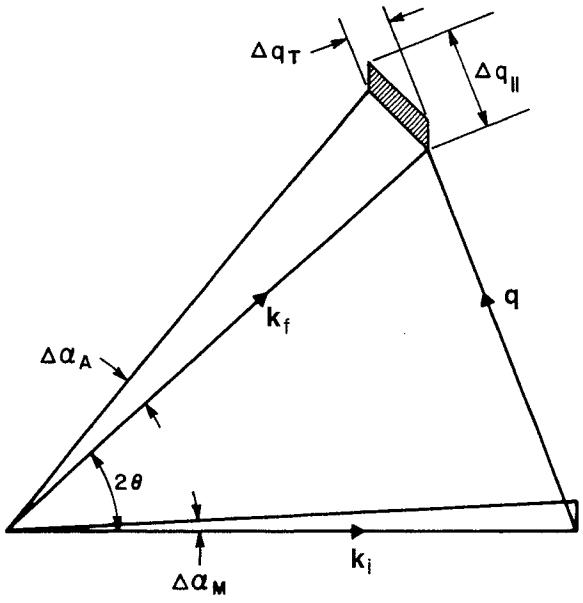

Figure 10d.1.4 Construction of the resolution function within the scattering plane of a diffractometer. From Robinson (1990b).

Surface Crystallographic Measurements

A subset of the general class of surface x-ray diffraction measurements is that pertaining to atomic structure determination alone. Here it is assumed that the surface under investigation is well enough ordered that the widths of all diffraction features are limited by the resolution function alone. This means that, in this case, any disorder that happens to be present is undetectable, and the surface is indistinguishable from ideal. It has been shown by Robinson (1990b) that in this limit the integrated intensity of the diffraction features is independent of the (unseen) disorder and so is representative of the crystallographic structure factor alone. Measurements of structure factors can then be analyzed in terms of the atomic structure of the surface, in

a close analogy to bulk x-ray crystallography described by Woolfson (1997) or Lipson and Cochran (1966).

If the disorder is visible in the form of peak broadening that is not too severe, it may still be possible to reach the ideal limit by deliberately worsening the resolution function. While it is often hard to control $\Delta\alpha_M$ since this is a function of the beamline optics, $\Delta\alpha_A$ can be opened up significantly by opening the 2θ detector slits. In all cases, the test for this desirable situation is that all diffraction features are resolution limited in their width. There are other limits in which the structure factor can be reliably measured if the peaks are significantly broader than the resolution function, then their peak intensity is representative of the square of the structure factor, provided a different, but calculable, correction is used.

The measurements needed for crystallography are most easily obtained by rocking scans of the principal diffractometer angle θ. In the detailed protocols below, the name of the θ angle known to the usual computer software is TH; these names will be cross-referenced where appropriate. This ensures that the narrow direction of the resolution function sweeps roughly perpendicular to the peak. If the peak is slightly misaligned, such a scan will usually catch it either earlier or later and still give the correct structure factor; this will not work if the misalignment is too severe, say more than two peak widths away, because, in general, there would be components of the misalignment in all possible directions. The use of a rocking scan is also prescribed by the definition of integrated intensity, the quantity coupled to the structure factor, as explained by Robinson (1990b) (see Appendix B). This corrects for all kinds of disorder, including mosaic spread, provided this is not too severe. It is also the most reliable way to estimate the background underlying the peak.

Grazing Incidence

It was explained (see Diffraction from Surfaces, above) that the use of grazing incidence orients the resolution function in a favorable direction for surface x-ray diffraction. This means that the incident beam, the exit beam, or both make a very small angle with the surface to be measured. This presents a special challenge in the diffractometry which is discussed below (see Practical Aspects of the Method). It also has other consequences.

The diffraction under grazing incidence conditions is no longer strictly kinematical because such a beam will partly reflect from the surface and also undergo a slight refraction as it crosses to the interior of the crystal. The effect, described by classical optics by Born and Wolf (1975), is small until the incidence angle α_i (or exit angle α_f) becomes comparable with the critical angle for total external reflection, α_C, which is of order a few tenths of a degree for most situations. When $\alpha_i < \alpha_C$, the beam is completely reflected from the sample and only an evanescent wave continues inside. This can be used to considerable advantage when extreme surface sensitivity is desired, since the typical penetration depth is of the order of 100 Å. Fortunately, Vineyard (1982) introduced a sound theoretical basis called the distorted-wave Born approximation for working with the effects of the critical angle. This approximation provides the grazing incidence method with great power.

The distorted-wave Born approximation has an additional consequence for surface x-ray diffraction: the intensity of the diffraction becomes modified under grazing incidence conditions. Born and Wolf (1975) show that the effect can be reduced to a simple transmission function for the intensity, $|T(\alpha)|^2$, as a function of either α_i or α_f, which accounts for the refraction effects. An example of calculations of $|T(\alpha)|^2$ is given in the upper panel of Figure 10d.1.5. As can be seen, there is a potential factor of 4 enhancement for both the incident and exit beams. The practical drawbacks with the factor of 16 are that it is only attainable when the collimation of both beams is severely restricted and the alignment is very difficult to achieve. The lower panel of Figure 10d.1.5 shows the effect of the distortion on the α_f profile of an in-plane bulk Bragg peak, which in the absence of the refraction effect would lie at $\alpha_f = 0$. Careful examination of the experimental curve can be used to identify whether the crystal diffracts from all layers up to its surface or whether there are inactive "dead" layers present, as shown.

PRACTICAL ASPECTS OF THE METHOD

An overview of the generic vacuum diffractometer configuration is given in Figure 10d.1.6. This instrument, which operates at beamline X16A at NSLS, is the most widely

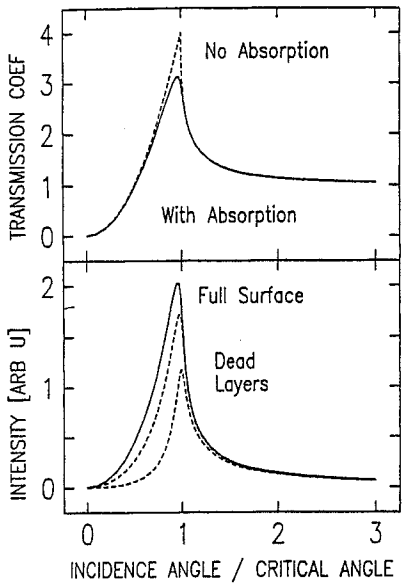

Figure 10d.1.5 Calculations of $|T(\alpha)|^2$ and the profile of an in-plane diffraction peak for gold at $\lambda = 1.5$ Å. The dashed curves show the effect of 5 Å and 20 Å of inactive dead layers of gold present above the crystalline part of the sample. Adapted from Dosch et al. (1991).

used design. All of the instrumental functions described in this section are generic to all installations of surface x-ray diffraction, although some specific details of the X16A instrument are given for clarity of illustration. Further machine-dependent details can be found below in the detailed protocols in the Appendices.

The overall size of the instrument in Figure 10d.1.6 is ~2 m long by 1 m wide and it resides at the beamline endstation. The instrument slides on air bearings, which allows it to be slid quickly into and out of the beamline hutch at the beginning and end of each experimental run. The configuration consists of an ultrahigh-vacuum (UHV) chamber (left side) coupled to a precision diffractometer. These two components will be described separately.

Vacuum System

On the left side, looking towards the x-ray source, lies the main vacuum chamber, which is used for sample preparation. It has turbomolecular (TMP), ion, and sublimation pumps (see *UNIT 1a.1*) located in a cross below the level of the main chamber. The TMP and ion pumps have gate valves that allow them to be isolated, for protection against power failure for the TMP and to reduce exposure to certain gases (e.g., Ar for sputtering and O_2 for dosing) for the ion pump. Numerous flanges are pointing at the sample, allowing the installation of various instruments for sample preparation and diagnosis. Samples are prepared by combinations of sputtering using an ion-bombardment gun, annealing by use of filaments, dosing with gases controlled by leak valves, and evaporation of substances using dosers. Dosers include commercial Knudsen cells and electron-beam evaporators, heated crucibles of molten materials, simple filaments coated with metal films, and getter-type alkali sources. Diagnosis is by means of LEED, Auger electron spectroscopy (AES; see *UNIT 11d.2*), and residual gas analysis (RGA). Most conventional surface science preparations can be carried out using combinations of these tools.

Most importantly, the capability of performing an x-ray diffraction experiment in situ is provided in the chamber. X rays can enter and leave the chamber through a semicylindrical beryllium window, shown in the center of Figure 10d.1.6. The window was brazed onto the vacuum wall at high temperature, so it is completely UHV compatible. It has 0.5 mm wall thickness so it transmits at least 95% of x rays with energies above 8 keV. In the diffraction position, the sample lies at the extreme right-hand side of the window with its flat face, upon which the surface has been prepared, facing left. The sample is rigidly connected to the diffractometer to the right. A manipulator wand located behind the diffractometer allows the sample to be detached from its rigid diffractometer mount and carried under UHV to the various instruments in the preparation chamber. There is a bellows and rotating seal coupling between the diffractome-

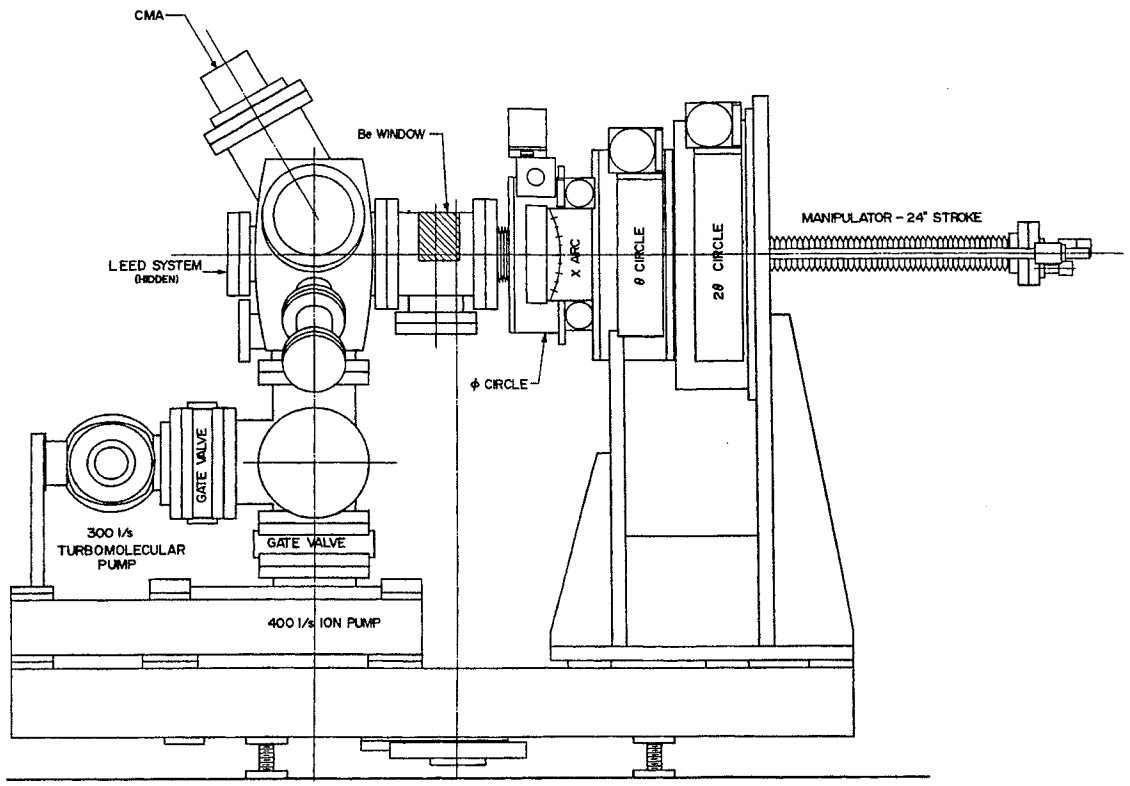

Figure 10d.1.6 Overview of the vacuum diffractometer configuration used at the X16A facility at NSLS by Fuoss and Robinson (1984). Other installations vary slightly from this design.

ter and the chamber, which allows the passage of the diffractometer motions. These last essential features were specifically designed for the surface x-ray diffractometer and so will be discussed next.

Because preparation of 10^{-10} Torr pressure is time consuming, a loadlock is used to allow simple manipulations of samples, thermocouples, and heaters to be carried out without venting the main UHV chamber. The basic principle of operation is shown in Figure 10d.1.7. For example, load locking is very useful for batch processing a series of samples or for introducing samples that cannot be baked at 150°C. Most instruments for surface x-ray diffraction provide some sort of load lock for rapid sample turnaround. Specific details for the operation of the X16A vacuum system are given later in the detailed protocol (see Appendix A), including the load-lock procedure, the venting procedure, and the bakeout procedure.

Sample Manipulator

Once it is retracted, the manipulator moves entirely with the sample on the diffractometer. A spring-loaded kinematical mount comprising three balls resting in 3 V-grooves 120° apart ensures that any flexure of the long arm of the manipulator is decoupled from the sample, which is thereby allowed to rest against the diffractometer ϕ axis. To carry the sample into the preparation chamber, the manipulator is extended by collapsing the 0.8-m-long bellows using a motor and gear on a threaded shaft. Electrical connections to the sample traverse the full length of the manipulator from its accessible rear flange. The last 75 mm of the shaft is illustrated in Figure 10d.1.7. It is crammed with intricate

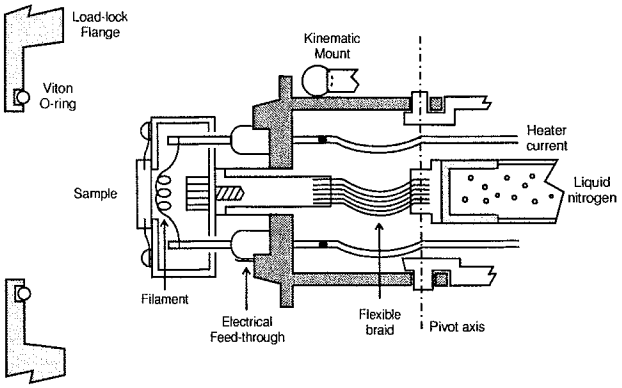

Figure 10d.1.7 Detail of the manipulator head shown in cross-section. The pivot allows the sample to point at 90° to the main axis to be presented to surface characterization instruments. The viton seal of the load lock, through which the sample is passed, is shown on the left. The mating surface is halfway down the manipulator head and contains vacuum feedthroughs for cooling and electrical connections to the sample. All parts to the left of this are accessible to the user during the load-lock procedure.

features that give it great versatility: a 90° elbowlike flexure driven by a push-rod running down the length of the manipulator that allows the sample to face the LEED and AES; a spring-loaded decoupling joint associated with the kinematic mount (not shown); a vacuum sealing flange penetrated by electrical and thermal feedthroughs for the load-lock system described below; and at the end 25 mm of clear space that allows the user to assemble his or her sample with the appropriate heaters, coolers, and sensors.

The rotating seal design is shown in Figure 10d.1.8. It allows the passage of rotations across the vacuum wall using a rigid shaft that has neither play nor backlash. It achieves this with three concentric sliding seals made of Teflon between which differential vacua are applied, the first stage at 10^{-3} Torr with a roughing pump, the second at 10^{-6} torr with a TMP pump. If any seal momentarily leaks during rotation, the pressure burst on the UHV side is minimized by the use of these differentials.

Five-Circle Diffractometer

The diffractometer geometry is illustrated with the aid of Figure 10d.1.9. This corresponds to a "five-circle" geometry, which was invented for surface diffraction by Vlieg et al. (1987). The standard names given to the angle variables describing the diffractometer setting are the same as the names of the axes in the figure. The principal axes are called (confusingly) θ and 2θ due to their association with the two-circle diffractometer setting describing Bragg's law. The symbols ϕ and χ are Euler angles of the sample with respect to the main horizontal (θ) axis. Finally α is the rotation of the entire instrument about the vertical axis. Historically at X16A, α was an afterthought, added to the instrument when it was found that the original four axes were too restrictive in their coverage of reciprocal space in the out-of-plane direction. Later instrument designs have incorporated α axes as a matter of course.

The convention for the zero settings of the axes is defined as follows: $\alpha = 0$ when the incident beam is perpendicular to the main horizontal (axis. The remaining definitions all correspond to $\alpha = 0$: $2\theta = 0$ (dial = 270 for the X16A instrument) when the incident beam strikes the center of the detector; $\theta = 0$ (dial = 270) when the χ axis lies exactly along the incident beam direction; $\chi = 0$ when θ and ϕ are collinear; and $\phi = 0$ is arbitrary and usually chosen to be the same as the mechanical dial setting. The names used by the usual computer program for these angular settings are TTH, TH, PHI, CHI, and ALP, as discussed below (see Appendix C).

The additional degrees of freedom over the four circles of a nonspecialized diffractometer are needed for two reasons: (1) the additional constraints on the diffractometer setting due to grazing incidence or exit conditions and (2) the limited range of the angles due to potential collisions with the vacuum chamber.

The χ axis is particularly affected by the second constraint since it is limited to ±10° at X16A by the coupling

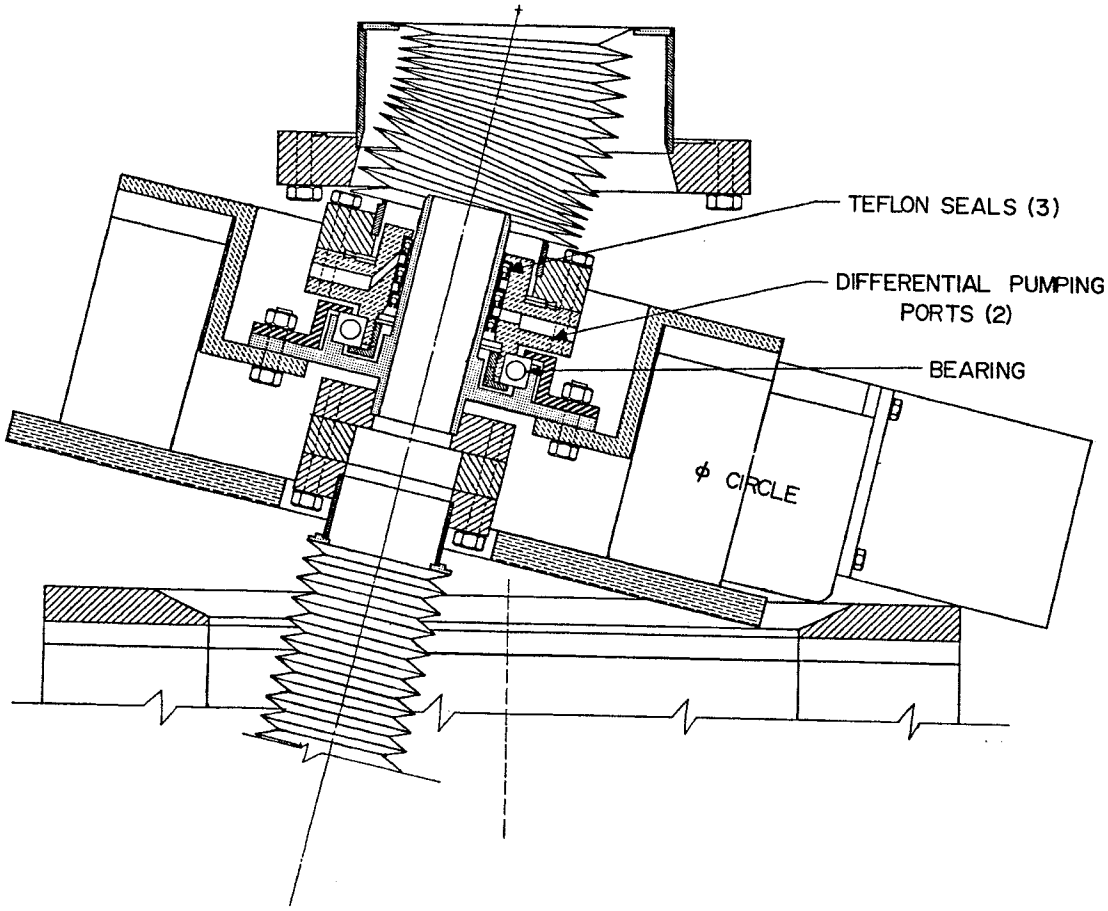

Figure 10d.1.8 Cross-sectional view of the bellows and rotating vacuum seal that couple the rigid motions of the diffractometer to the sample in UHV. From Fuoss and Robinson (1984).

bellows and also by the manipulator. There is also a "six-circle" geometry due to Abernathy (1993) with an extra angular out-of-plane degree of freedom for the detector, called GAMMA, a "Z-axis" geometry due to Bloch (1985) that is a subset of six-circle geometry without the ϕ and χ motions, and also a "2+2" geometry used for surface diffraction by Evans-Lutterodt and Tang (1995).

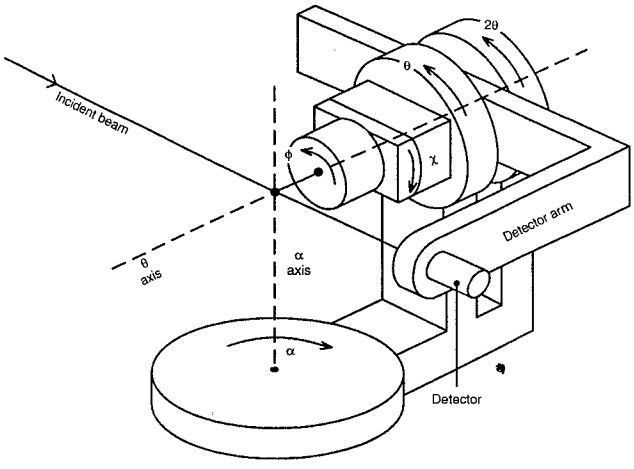

Figure 10d.1.9 Isometric view of the five-circle diffractometer. The names of the axes and their positive directions of turning are indicated.

Laser Alignment

Many of the typical measurement methods of surface x-ray diffraction employ the grazing angle geometry (see Principles of the Method) on the incident beam, the exit beam, or both. It is therefore crucial that the physical orientation of the sample's surface be well known. To allow for the general case (rather commonly occurring) that the surface orientation is not a simple crystallographic orientation, perhaps due to miscut, it is important that the optical surface orientation be defined independently of the crystallographic orientation. This step is known as "laser alignment."

A laser beam is directed roughly down the main (θ) axis of the instrument and reflected from the polished sample surface and allowed to strike a screen located behind the laser. If the θ axis is rotated, the reflected spot will precess in a circular orbit. The center of this circle is the correct laser reflection angle if the sample face were exactly perpendicular to the axis. The beam can then be directed onto this center by adjustment of the diffractometer ϕ and χ angles until the laser spot remains stationary upon rotating

θ. These settings, called fphi and fchi in the detailed protocol below (see Appendix C), are then a unique representation of the sample's optical orientation and are entered into the diffractometer control program so that the incident and exit angles can be precisely controlled.

Sample Crystallographic Alignment

Sample alignment is normally achieved by finding the diffractometer settings for diffraction from a small number of bulk Bragg peaks. If the lattice parameters are known, a complete orientation matrix is specified by the positions of just two Bragg peaks using the method of Busing and Levy (1967). If the lattice parameters are not known, it is necessary to specify the positions of at least three non-coplanar Bragg peaks. The orientation and calculation of arbitrary settings will be made by the control program once this information has been furnished.

The usual procedure for locating the Bragg peaks is to manually vary the diffractometer angles to maximize the diffracted intensity. This is less straightforward with a five- or six-circle diffractometer than with the more standard four-circle instrument, simply because there are more degrees of freedom in which the user can get lost. A reflection has 3 degrees of freedom, so the five-circle diffractometer has two motions too many. In particular, the detector moves on two axes, one of which (α) also moves the sample: there is no longer a simple connection between Bragg's law and the detector motion. Here are some guidelines on the suggested method of finding peaks:

1. Set up a "dummy" orientation matrix (OM) with the best known values of the lattice parameters (see Appendix C). Two mutually perpendicular in-plane reflections can be specified as having the laser orientation angles. From here, the setting of a suitable bulk out-of-plane Bragg peak can be calculated. In-plane peaks are hard to find because both incident and exit beams must be exactly grazing; out-of-plane peaks have a much wider choice of possible settings. Set the diffractometer at that position.

2. The desired reflection can be found by rotating the sample about its surface normal using either ϕ or θ. The peaks are so strong with synchrotron radiation that the motors can be searched at top speed; the reflection will "flash" on the detector oscilloscope or rate meter. There is usually sufficient thermal diffuse scattering (TDS) for a peak to be found in this way, even when it is several degrees away from the line that is searched.

3. Ride up the TDS until the center of the Bragg peak is found. Diffracted beam attenuators will be needed at this stage. Centering can be quickly and automatically carried out with "line-up" (lup) scans of a single motion (see Appendix C), after which the program calculates the center of mass and sends the motion there.

4. When using a PSD with an entrance window that is wide along the q_z direction, the peak may appear at any position along the length (q_z). Since the diffractometer is aligned to the center point of the detector, the contents of the PSD in the MCA must be viewed (function key F1 or F2) and the peak made to walk to the center. Alternatively, a region of interest should be defined about the center and only the counts in this region used for reflection centering.

5. Once a peak is centered, it is better to rotate the dummy matrix manually to the corresponding orientation. This way both defining reflections are rotated together. If merely one of the reflections is overwritten, the resulting two-peak orientation matrix may be very unrealistic and will make it hard to find the second peak. Alternatively, the second dummy reflection can be chosen to coincide with the surface normal direction.

Once two peaks are found, the orientation matrix is complete and can be used to find any further points in reciprocal space. There will always be small errors of both crystal and diffractometer alignment, which may accumulate and result in poor prediction of further Bragg peaks. There are two ways of avoiding this problem:

a. Use alignment peaks that are most relevant to the features to be measured. For example, a good alignment for measuring a CTR would be to choose two Bragg peaks through which the rod passes.

b. Use multiple-peak alignment. Diffractometer alignment errors can be partially compensated by using the crystallographic unit cell parameters as free variables. An excellent orientation matrix will always be obtained by using a least-squares refinement of the best lattice passing through many Bragg peaks, especially if they are at large diffraction angles.

DATA ANALYSIS AND INITIAL INTERPRETATION

The following summarizes the different ways to present surface x-ray diffraction data to express one or other sensitivities or strengths of the technique. Different material properties of a given surface or interface would require entirely different kinds of measurement to be made. Each subsection lists a different form of presentation of the data that the reader might encounter in the published literature, then describes the typical measurement involved, and finally cross-references the typical diffractometer scans (Appendix C) and typical data analysis steps (Appendix B) that might have been followed. At the end of the section, a worked example is given.

Rod Profiles

Crystallographic measurements referred to above (see Principles of the Method) are used for surface and interface structure determination. The same procedures apply to CTRs or superstructure reflections. The general form of the data is to convey the magnitude of the structure factor along a line of points in reciprocal space, running along a line perpendicular to the surface. Theta-rocking scans (see Appendix C) are taken at a range of q_z values or Miller index L. These are numerically integrated and background sub-

tracted, e.g., using the program PEAK (see Appendix B). For reliability, it is essential to measure multiple reflections related by the surface symmetry. When these symmetry equivalents are merged together, e.g., using the program AVE (Appendix B), their reproducibility is thereby determined and then used to specify the experimental error in the structure factor magnitude. Further details, including the equations defining the error estimate are given by Robinson (1990b).

The data are usually plotted as smooth curves against the perpendicular momentum transfer, L. Since the structure factor is a continuous function, enough L points must be measured to be sure that the profiles are smoothly varying and that all oscillatory features are resolved. This last caution is particularly apt in the case of thin films, which have many closely spaced thickness fringes; in this case, some researchers choose to simply scan along the q_z ridge of intensity in a "direct rod scan" and then to offset the θ angle and repeat the scan to estimate the background.

The rod profiles are then fit to the functional form of the structure factor of an atomic model of the surface, as outlined above (see Principles of the Method). In the kinematical limit, both for CTRs and superstructure rods, this is given by a complex linear sum over atoms representing the superposition of atomic form factors. Closed-form expressions are needed for the form of the CTRs to account for the infinite sum. The surface roughness must also be accounted for at this stage. The program ROD, written by E. Vlieg and described in Coppens et al. (1992) (see Appendix B), is a widely used computer program for this purpose. Atomic models of bulk and surface regions are specified in parametric form in a very general format. The parameters of the model are then refined by a least-squares minimization to give the atomic coordinates on the model.

It should be noted that surfaces are very different from bulk matter in the specification of atomic models. Each layer of the structure is expected to have a different Debye-Waller factor representing its atomic vibration amplitude. These Debye-Waller factors usually increase significantly in magnitude in passing from the bulk outward in the structure. Another common feature of surfaces is partial occupancy of lattice sites. It is also common to find more than one site, each partially occupied, for a structure with disorder. All of these situations are handled by the ROD program (see Appendix B). Finally, surface atoms are prime candidates for anharmonicity, since they have neighbors on one side but not the other. Surface anharmonicity has been analyzed in the pioneering work of Meyerheim et al. (1995).

Reflectivity

The specular reflectivity is the special case of the CTR emanating from the origin of reciprocal space. While it can be measured in the way described in the previous section, this can also be achieved with the simple two-circle method if the sample is mounted perpendicular to the θ axis. It is customary to plot reflectivity data as the square of the reflection coefficient versus total momentum transfer, q_z. This gives a normalization to the data different from the crystallographic standard described above: an ideally terminated surface would have an intensity dropping as q_z^{-4} in these units, according to the Fresnel law of reflection. To emphasize the differences, the reflectivity divided by the (calculated) Fresnel reflectivity is often what is plotted. There is a correction for the total external reflection region at small angle, which can be understood with a simple dynamical treatment.

Als-Nielsen (1987) has derived a "master formula" for the analysis of reflectivity data in terms of the spatial derivative of the electron density profile of the surface. When q_z is small, the resolution is insufficient for atoms or atomic layers to be located, so the electron density is parameterized as a series of slabs of variable density connected by error function shaped transition regions of variable width. These parameters are then refined by least squares to fit the data and obtain the electron density profile explicitly.

Reflectivity is the method of choice for measuring the sharpness of the layer profiles of artificial multilayer structures that are chemically modulated by varying their composition during deposition. Thick multilayers of electron-dense materials require a full dynamical treatment for correct analysis, in which transmission and reflection coefficients of each layer interact self-consistently. The theory was worked out by Parratt (1954) and has been implemented by Wormington et al. (1992). It is also commercially available as a software product called REFS from Bede Scientific.

Surface Diffuse Scattering

Surface roughness can be measured quantitatively using the CTR profiles, as mentioned above (see Principles of the Method). It is also measured routinely by the reflectivity method above. In either case, the intensity that is missing from the CTR or the reflectivity, resulting in a lower signal, reappears as diffuse scattering nearby. This was clearly explained in terms of the lateral correlations associated with the roughness in an important paper by Sinha et al. (1988).

The surface diffuse scattering can be measured most easily near the origin of reciprocal space by means of wide θ scans (see Appendix C). Such scans have several characteristic features that have simple interpretations: in the center there appears the CTR or the specular reflectivity as a sharp spike; at the two ends of the scan lie the "Yoneda wings," where the diffuse intensity rises by the $|T(\alpha)|^2$ transmission function as $\alpha_i \approx \alpha_c$ or $\alpha_f \approx \alpha_c$; in between lies the surface diffuse scattering. Multilayer samples are found to have rich surface diffuse scattering patterns that provide information about the correlations between the positions of the various layers making up the multilayer.

Reciprocal Lattice Mapping

In some surfaces undergoing phase transitions or morphological changes, there is valuable information in just the diffraction peak positions, widths, and intensities. For example, surface diffraction is extremely sensitive to the appearance of new periodicities in surfaces, and this has been exploited extensively. The measurement consists of recording wide scans, e.g., using the *iscan* and *jscan* described below (see Appendix C), along simple directions of reciprocal space. Such curves would be plotted as a function of temperature, time, or other control variables. Sometimes two-dimensional scans (*kscan*) are also made to map out all the identifying features. A crystal analyzer, which provides much higher **q**-resolution, may be needed to separate finely spaced features.

The materials properties of interest that can be derived from such measurements concern grain shapes and sizes and the degree to which these are strained. The positions of Bragg peaks in any diffraction experiment determine the lattice parameters of the sample crystal; e.g., high-resolution x-ray diffraction is probably the most accurate of all and can achieve 1 part in 10^5 using the Bond method. Such measurements provide information about strain and its distribution within the sample. Similarly, accurate measurements of diffraction line widths, through the Scherrer formula, determine the size of the diffracting grain. In both these situations it is routine to use a careful lineshape anaylsis to extract the most reliable sample parameters. The semi-automatic program ANA described below (see Appendix B) provides a battery of possible lineshapes that apply to different kinds of diffracting objects or distributions of objects.

Grazing Incidence Measurements

Grazing incidence measurements fall into two categories. The first is a simple extension to all of the above techniques to determine materials properties as a function of depth inside a sample. Grazing incidence of exit conditions is then employed to vary the penetration depth into the bulk, which can be calculated reliably from the known refractive index and absorption values of the material at the x-ray energy used. The distribution of depths sampled is always exponential, so it is never possible to select a particular depth of interest; for this purpose it would be necessary to use a nonlinear technique such as ion scattering (see Chapter 12). Dosch (1992) has suggested the use of Laplace transforms to deconvolve the depth information.

Since the incident and exit angles always have to be under control in a surface x-ray diffraction experiment, it is a routine extension of the normal procedure to deliberately control them. For example, with the diffractometer control program "super," the penetration depth can be chosen by setting the target value of the incident or exit angle, α_i or α_f (B or B2 in Appendix C). A useful extension is to make a *vscan* at a fixed reciprocal lattice position as a function of α_i or α_f.

The second category of grazing incidence measurement is to use the PSD to record an entire α_f profile in a single measurement. This method was pioneered for the study of surface-phase transitions in a depth-resolved way by Dosch (1987, 1992). It has the advantage that diffractometer motions are not required during measurement of small changes with temperature. More recently the method has been improved by Salditt et al. (1996) to record and analyze diffuse scattering from multilayer samples as a function of exit angle α_f in a PSD by making wide θ scans at fixed α_i.

Worked Example: the Si(111) Surface

When the bulk crystal has a sufficiently simple structure, in the case of all primitive crystal structures, or the NaCl structure, there is only one possible way to cut the lattice to reveal a surface. However, in this case, the CTR presented above (see Principles of the Method) is technically indistinguishable from a simple superposition of $1/q^2$ intensity tails around each Bragg peak, as discussed by Robinson (1990a). Whenever the crystal has a multiple-atom basis that allows for more than one possible termination, the shape of the CTRs depends on which termination exists and is then clearly distinguishable from the superposition of $1/q^2$ intensity tails.

Such is the case of Si(111), where two possible terminations can exist, as illustrated in Figure 10d.1.10. The double-layer (D) termination occurs when bonds perpendicular to the surface are cut; the single-layer (S) termination occurs when we break the bonds inclined at 19° to the surface, as shown. The density of dangling bonds is three times greater for the latter case, so it might be considered less likely to occur. The calculated CTRs are plotted for the two cases in the lower half of Figure 10d.1.10. Up to a factor-of-10 difference in the two structure factors is seen to occur.

In reciprocal space, the specular reflectivity line is the direction with the momentum transfer, **q**, entirely perpendicular to the surface. This corresponds exactly to the

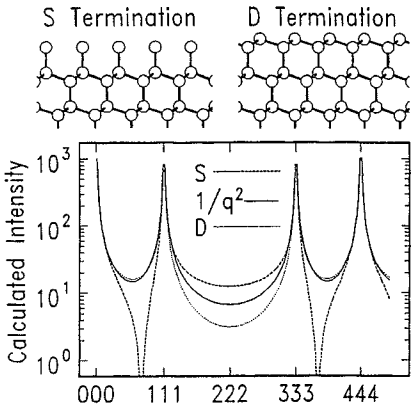

Figure 10d.1.10 Top: the possible S and D terminations of the Si(111) surface. Bottom: calculated specular reflectivity for the two terminations according to the CTR theory and by superposition of $1/q^2$ intensity distributions.

zeroth-order CTR diffraction and so can be thought of as a CTR; the analysis of these data is particularly simple because only the vertical components of the atomic coordinates enter, by virtue of the section-projection theorem of Fourier transforms. The question, then, is how is the real Si(111) surface, prepared in UHV, terminated? This is complicated by the fact that it is reconstructed with 7×7 translational symmetry.

Example of Measurements from Si(111)7×7

Figure 10d.1.11 shows the measurements of the specular CTR of Si(111)7×7 using an improved data collection method. An x-ray PSD was placed so that it cuts across the diffracted beam. The background is then measured simultaneously with the integrated intensity of the diffracted beam and can be immediately subtracted. It is clear from the data that neither the S nor D simple termination adequately describes the surface. The figure also shows the result of a least-squares fit to the data, which passes through the points respectably well. The model used was the dimer-adatom-stacking fault (DAS) model for the Si(111)7×7 reconstructed surface due to Takayanagi et al. (1985). The heights of the atoms and the vibration amplitudes in the top four layers were adjusted for a good fit using the program ROD described in Appendix B.

Figure 10d.1.11 also shows an additional sharp feature in the center of the scan at the position of the specular 222 Bragg reflection. This is indeed the specular 222 Bragg reflection, which is forbidden in diffraction from the ideal diamond lattice but is not perfectly extinguished for two reasons suggested by Keating et al. (1971):

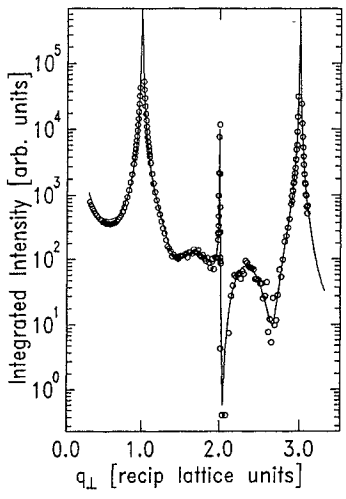

Figure 10d.1.11 Measured x-ray reflectivity of a UHV-prepared Si(111) sample using a PSD. The solid line is the least-squares fit to a model based on the DAS model for the 7 × 7 reconstructed surface due to Takayanagi et al. (1985). From Robinson et al. (1994).

1. The vibrations of the ions in the lattice are not spherically symmetric but tend to bulge out along the tetrahedral directions (four of the eight {111} directions) opposite to each bond; the anisotropy is along different directions for the two atoms in the basis, meaning they are crystallographically inequivalent.

2. The electrons forming the sp^3-hybridized bonds between the Si atoms are not spherically symmetric either but have a tetrahedral shape, again meaning the two atoms are crystallographically inequivalent. This affects 4 of the 14 electrons in the Si form factor so it is a relatively large effect.

It was shown many years ago by Keating et al. (1971) that contribution 1, which is temperature dependent, is dominant in neutron diffraction, while contribution 2 is more important in x-ray diffraction experiments. We therefore included extra bond charges in our model to fit this 222 peak in our data. It is orders of magnitude weaker than the bulk diffraction but still stronger than the surface component of the CTR. A particularly noteworthy feature is the interference between the tails of the 222 and the CTR.

PROBLEMS

This section is a critical appraisal of the weaknesses of the surface x-ray diffraction technique. It might be used in evaluating published work, e.g., in searching for alternative explanations of results obtained with the method.

Surface Crystallographic Refinement

Crystallography has an inherent "phase problem." It is the structure factor amplitudes that are measured, not the phases. The solution of an atomic structure amounts to testing hypothetical models for agreement with the measurements. It is assumed that a good fit will only occur for one model, which therefore finds unique values for the missing phase information.

The difficulty with this logic is that it depends upon the quality and quantity of the data. For good, numerous data, experience has shown that there is usually a unique solution. In fact, many researchers are frustrated by the situation that they cannot find a model that agrees with their data! This is a heuristic support for the notion of uniqueness. "Direct methods" of structure solution, which exist for small-molecule crystallography (Woolfson, 1997), are being developed for surfaces but are not yet ready for widespread use.

The problem arises when there are insufficient data for the solution to be determined. The accepted rule of thumb (Lipson and Cochran, 1966) is for the structure to be overdetermined by a factor of 3:1. This means that for every structural degree of freedom in the model, there must be three independent measurements. It is presumed that nonuniqueness of the solution would be extremely unlikely when three separate measurements must all agree with each other for every parameter determined. For this to work, the counting must be done honestly: we will consider first the

question of counting model freedoms and then that of counting the data.

It is possible to tie structural parameters together to reduce the degrees of freedom, but this always requires assumptions or constraints on the possible structures that might exist. Chemical constraints such as bond lengths and angles are usually safe, but sometimes unorthodox chemistry can take place at surfaces. This is often done through a Keating model (Keating, 1966) where a penalty for nonstandard bond lengths and angles is added to the χ^2 functional used for least-squares minimization. Another common constraint is to collect the less-sensitive parameters, such as Debye-Waller factors, into groups applying to several related atoms. Yet another constraint is to enforce exponential decay of relaxation parameters from the surface toward the bulk; this amounts to assuming the form of the solution of the Poisson equation describing continuum elasticity in the material. In each case, if the hypothesis leading to the constraint is questionable, then the conclusions drawn are questionable.

A similar logic concerns counting the data. This relates also to their accuracy, which can be measured in the way described above (see Practical Aspects of the Method). The situation is more complicated for surface than for bulk crystallography because the data are in the form of "rod profiles," which are continuous functions of L. The amount of information in a given rod profile can be counted, but this must be done carefully: every distinct maximum and minimum in the rod counts as one independent data point. Whether or not an extremum is distinct is closely tied to the size of the error bars of the measurement.

In principle, all error analysis should be handled through the definition of the normalized χ^2 functional, which is weighted by a factor $1/(N-P)$, where N and P are the number of data and number of parameters that we have just defined. The danger is that, while P is usually correct, N is frequently overestimated because it counts separately all the data points along each rod, rather than just the number of extrema. Nonspecialists and specialists alike quote a small goodness of fit χ^2 (near 1.0) value as an endorsement of the correctness of a structure. This is nonsense! A small χ^2 simply means that the data have been exhausted and the model is sufficiently detailed; it does not necessarily mean it is right. An easy way to obtain a small χ^2 is to measure very few data!

In examining published work, there are certain indications that the refinement of the structure had been difficult. Debye-Waller factors are sometimes omitted because they refine to negative values when included. Negative Debye-Waller factors are unphysical and so usually indicate some other deficiency in the model. Another bad sign in a structural model is when many atoms with partial occupancy have been included. Partial occupancy is common on surfaces, because of their nature: when a crystal is cut, it must have a boundary, but not necessarily one with an ordered structure.

Other Surface Crystallography Problems

Regarding the question of the quality of structure factor data, some aspects are specific to the case of surfaces. Apart from gross misalignments, there are subtle ways that additional errors can be introduced. When grazing incidence is used, the slightest variation of α_i from one measurement to the next causes a different value of the $|T(\alpha)|^2$ prefactor and hence the observed structure factor. In an extreme case, misalignment can cause α_i to become negative and the beam to disappear below the horizon. Sample curvature can aggravate the problem, leading to a different distribution of α_i values along different incidence azimuths. The only safe way to avoid the problem is to measure symmetry-equivalent reflections and record the data reproducibility.

When CTR data are included, there are several dangers associated with measuring very close to bulk Bragg peaks. Highly structured background is commonly found and must be carefully subtracted. The problems are compounded when the out-of-plane detector resolution is opened up to improve counting rates. There can be a significant distortion of the data from the L variation of the intensity across the detector slit. The safest strategy is to avoid including data near the Bragg peaks, except where absolutely necessary.

Another problem can arise from unavoidable beam harmonics. The detectors are not always capable of discriminating $\lambda/3$ (and $\lambda/4$, etc.) contributions completely. This means that any measurement at or near an integer fraction of a bulk Bragg peak can give a strong "glitch." For simplicity, it is common to avoid all measurements at small-integer fractions of L.

A different source of possible misconception concerns symmetry. There are many cases of published work where the surface structure has lower symmetry than that of the underlying bulk crystal. For example, all reconstructed surfaces have lower translational symmetry than the bulk, and this is accepted for chemical reasons. The general rule is that a surface structure should have as high a symmetry as possible, compatible with the symmetry of its parent bulk. Only when this is shown to be impossible should the symmetry be broken. Then one symmetry element at a time should be removed from the model, since each symmetry that is lost can greatly increase the number of degrees of freedom.

A common source of confusion is that the symmetry of a surface is not immediately obvious from the symmetry of the diffraction pattern. Domain formation is common on surfaces, where differently oriented regions nucleate in different locations. It is usual to average the intensity contributions from each of the orientational domains, rather than the structure factor. This amounts to the assumption that the domains are far apart, beyond the coherence length of the measurement. The opposite limit of microdomains within the coherence length is usually apparent from a broadening of the peak lineshapes. This can be handled by mixed structures with partial occupancy once the peaks have been integrated correctly to account for their enlarged widths.

Lineshape Analysis

The purpose of analyzing lineshapes is to extract parameters that relate to materials properties so that they can be tracked as the sample is varied in some way. It is usually the peak position and/or width that is of interest. Typically the fitting is done directly to the output data stream in a semi-automatic way, e.g., using the program ANA described in the detailed protocol in Appendix B. If the curve that is used for fitting has the wrong shape, systematic errors will be introduced that may or may not have consequences. For this reason, a battery of lineshapes is usually available, sometimes with several adjustable parameters. A good example of a generally useful lineshape is the Lorentzian function raised to a power:

$$p(x) = A[(x-B)^2+C^2]^{-D} \quad (2)$$

where A, B, C, and D are adjustable parameters (B and C are the position and width most often sought). The danger here is that of parameter coupling or nonorthogonality, particularly between parameters C and D. If D is just allowed to vary from one fit to the next, and then later ignored, unwarranted changes in C may occur that are not really present in the data. Here, the solution is to find a value of D that applies to most of the data, then fix the parameter for fitting the data series to look for the trends.

A different situation applies to the handling of background, which is seen as a nonvanishing intensity in the extension of the tails of a peak. The background is due to unwanted additional scattering sources within the sample or the instrument. Usually the background is subtracted by extrapolation. The background can have a profound effect on the stability of fitting lineshapes such as the Lorentzian function raised to a power above, especially if D is the parameter of interest. The best advice here is to measure a lot of background extending far away from the peak; this has a surprisingly beneficial effect in constraining the fits of functions with long tails such as this.

The best procedure for measuring diffuse scattering is again to control and understand the background. By its nature, there is no perfect way to separate diffuse scattering from background. The most difficult situation is that of small-angle scattering near the direction of the incident beam, which applies to the nonspecular reflectivity region for surfaces discussed above (see Data Analysis and Interpretation). Here, the potential sources of background extend all the way back up the beamline to the entrance slits and beyond. A common hazard in diffuse scattering measurements is the tails of the resolution function, which appear to be CTRs pointing in apparently unusual directions. In fact, they are the CTRs of the crystals in the monochromator or analyzer rather than those of the sample!

DETAILED PROTOCOLS

The exact procedure will vary slightly from installation to installation, but the general principles will be the same. To be specific, we discuss here the procedure for the X16A surface diffractometer at NSLS. The generalization to other installations will usually be obvious. Details of the vacuum procedure are given in Appendix A, the data analysis programs in Appendix B, and the diffractometer control program in Appendix C.

Alignment of the Beamline

The X16A beamline, like many others used for diffraction, consists of a grazing incidence toroidal mirror and double-crystal monochromator. It is the responsibility of the NSLS facility staff to help the user get to the point of operating the beamline. This requires verification of all safety-related hardware on a "safety checklist" and that the condition of all cooling and vacuum systems be "green" before the safety shutter will open.

The mirror focusing is 1:1 and so should produce a focal spot on the sample ~1 mm wide by 0.5 mm high. The focal length is fixed and requires the correct incidence angle of 5.65 mrad, which fixes the final height of the focused beam. It is important to ensure that the height is correct by using a focusing screen near the sample position and a TV camera with a close-up lens. The beam image is a U-shaped "smile" when the incidence angle is too low and an inverted smile when the incidence angle is too high. The locus of focal images traces out an X shape on the screen upon tilting the mirror, with the optimum focus at the intersection of the X. A tilted smile means the mirror is not steered correctly and requires rotation about the vertical axis. The mirror bend should then be adjusted for the smallest vertical profile, and the beam position should be scanned to verify it is not being cut by any nearby aperture edges.

The double-crystal monochromator is controlled by five manual adjustments. The energy is set by a stepping motor on the back of the tank that is driven by a manual pulser. This can also be controlled by pulses from the beamline computer if needed. The energy reading is a dial counter, which is converted to kilo-electron-volts on a chart in the beamline log book. The θ and χ angles of each crystal are controlled by stepper motors driven by a shaft-encoder knob and selected by one of the four red "engage" buttons. The four angles are also read out by absolute encoders. It is very important not to move these in-vacuum motors far from their starting positions because there are no limit switches. After changing energy, it is necessary to bring the two crystals parallel again by adjustment of θ_2 until a signal is seen in the ion chamber. Side-to-side steering of the beam position is achieved by χ_1,which is generally used to bring the beam onto the sample (see below).

The monochromator feedback circuit is shown in Figure 10d.1.12. The second crystal is modulated at 200 Hz by a piezoactuator. When its rocking curve is correctly centered on that of the first crystal, the lock-in amplifier reads zero output; if the angle is misset, a positive or negative error signal is generated that corrects the angle. The loop gain and integration time may have to be adjusted for correct

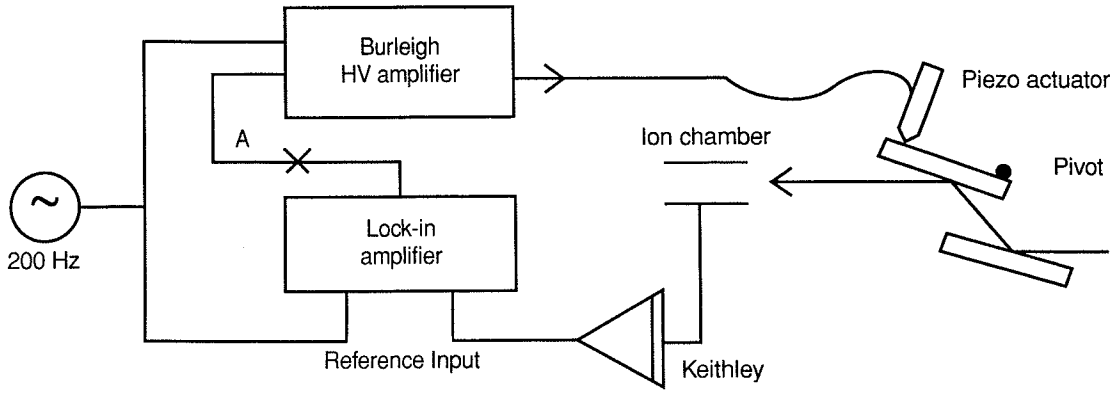

Figure 10d.1.12 Monochromator feedback circuit. Point A is where the feedback loop should be broken in order to detune the monochromator.

performance. To detune the monochromator (e.g., to remove harmonics in the beam), the loop must be broken at point *A* and the crystal angle set manually.

Alignment of the Diffractometer

The intersection of the five axes of the diffractometer is at its center, and this must be positioned accurately on the beam's focal spot. This must be correct to within 100 μm. The beam direction must also be perpendicular to the θ and α axes to within 0.1° and 0.3°, respectively. Because a surface x-ray diffractometer has a sample in a UHV environment also at its center, this presents a special challenge.

The vertical position is set by four screw jacks under the diffractometer table. These are manually or stepping-motor driven in two pairs, front and back, to allow the table to be tilted until the beam is perpendicular to the α axis. The tilt is equal to the beam's known 11.3 mrad angle to the horizontal and preset using a spirit level and rulers. The horizontal position is set coarsely using surveying marks and finely by moving the beam with the χ_2 monochromator adjustment. The perpendicularity of the theta axis is determined by the choice of the zero of α.

The essential alignment tool is an "off-axis pinhole" that is an L-shaped bracket with a 1-mm pinhole drilled through it. This bolts onto the ϕ circle of the diffractometer so that it wraps around the outside of the UHV chamber and presents itself to the incoming or outgoing beam, as shown in Figure 10d.1.13. The distance from the pinhole to the mounting surface is accurately machined so that it corresponds to the manufactured radius of the χ arcs. Because of its offset from the center, the position of the pinhole with respect to the beam is scanned by moving the ϕ and χ axes of the diffractometer.

Because the sample is blocking the true center position so that the x-ray beam cannot pass, the alignment must be carried out at a controlled location just above it. This is done by tilting the diffractometer χ by a known amount (usually 1°) from its calibrated zero and moving the beam with the χ_2 (monochromaor) to correspond. The center position of an arbitrarily placed starting beam is determined in (ϕ, χ) space with the pinhole on one side of the sample and then again on the other side. An exact 180° rotation of θ takes the pinhole from front to back, as shown in Figure 10d.1.13. Half the difference between the two ϕ values multiplied by the lever arm *L* is the error in the table height, which is thereby corrected. Half the difference between the two χ values is the deviation of the beam from perpendicularity with the θ axis, which defines the zero of α.

Once these corrections have been made, the pinhole is exactly aligned with the diffractometer center, offset horizontally to avoid the sample. The beam, passing through the pinhole, can then be used to set precisely the vertical incident and exit beam collimation slits. If the pinhole is

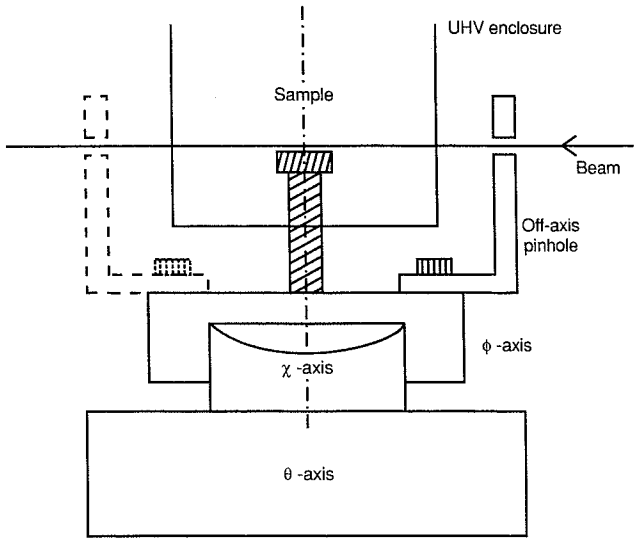

Figure 10d.1.13 Off-axis pinhole designed to mark the center of the diffractometer without breaking the vacuum. The dashed position is reached by a 180° rotation of the θ axis.

then removed and the beam moved until it grazes across the sample at the center, the horizontal slits can be set too. This is also the opportunity to set up the channel definitions of the PSD (if used), by marking off known distances from the calibrated center line.

The centering of the α axis with respect to the other four is also adjustable, owing to its historical origin as an auxiliary sample motion. The adjustment is by means of a motorized linear translation across the beam and slotted screw-holes in the direction parallel to the beam. Previous settings of these adjustments are recorded in the logbook, and these should be used as starting values. The alignment should not be needed often as the performance does not depend critically upon it; the usual symptom of misalignment is a loss of intensity at large values of perpendicular momentum transfer. It is carried out using the off-axis pinhole once this has been centered exactly on the beam following the procedure above. Then θ is rotated by exactly 90° so that the pinhole is pointing straight up, thereby marking a point exactly above the intersection point of the axes, as can be seen in Figure 10d.1.9. The center of the α axis is then brought to intersect this marked point by using the translations. This is most easily performed with a high-magnification TV camera hanging down from the hutch roof: when α is rotated by hand, the pinhole position should be invariant.

Angle Calculations

The principal purpose of the diffractometer control program is to make the angle calculations that map the reciprocal crystal coordinates onto the angle setting of the diffractometer. This calculation depends on the mode of operation of the instrument, which is the "five-circle" mode for the installation discussed here. The program also contains the software drivers for the axis motors corresponding to the diffractometer angles so that these can be moved by the program. It also generates the most useful kinds of scans automatically and keeps track of the orientation matrix. Its other major task is to produce the output files that contain the results of the experiments organized in a readable format. Here we make reference to the diffractometer control program "super," but many of the basic principles are common to other programs, e.g., the commercial "spec" program used elsewhere and available from Certified Scientific Software. Details of the command structure of "super" are included in Appendix C.

Angle calculations in the five-circle mode are described in a paper by Vlieg et al. (1987). The diffractometer has 5 degrees of freedom in the most general five-circle mode (alm = 2) and 4 degrees of freedom when alm = 1 (see Appendix C, Basic Super Variables). Three of these are needed to select a point of measurement in (3D) reciprocal space; one more is used to constrain the incidence or exit angle (see bem in Appendix C, Basic Super Variables). The 5th degree of freedom is used to help control the resolution function, bearing in mind that the diffraction features to be measured are highly elongated into "rods" along the direction perpendicular to the surface: the program arranges for the crystallographic c^* axis to lie in a horizontal plane. When the diffraction rods (assumed parallel to c^*) are horizontal, the vertical high-resolution direction lies exactly across them.

The constraints on the five-circle diffractometer will allow inclination of the incident beam (ALP), but not the exit beam (GAMMA), from the sample plane. Because of the limits on CHI, the sample must lie within some degrees from perpendicular to the main TTH/TH axis. A consequence of these constraints is that most reciprocal space is accessible only in the bem = 2 mode (see Appendix C, Basic Super Variables) in which grazing exit conditions are maintained. This has the advantage that the PSD can then record the exit beam transmission profile for all reciprocal lattice settings. The exit angle (set by the variable B2) arises from setting TH near TTH + 90° and tilting CHI to a value near the negative of B2, as can be seen with the aid of Figure 10d.1.9. The exact values depend on how close the "laser alignment" (see Practical Aspects of the Method) angles are to the ideal flat setting, fchi = 0. For this reason the θ axis should be expected to work roughly in the range 90° < TH < 150° and the limits should be set to accept this range, e.g., –30° < TH < 150°.

ACKNOWLEDGMENTS

It is a pleasure to thank the various people who have helped develop this technique and the X16A facility over the past 15 years. Paul Fuoss helped develop the beamline and original surface diffractometer hardware. Elias Vlieg invented the five-circle mode and wrote the data analysis programs. Robert Fleming wrote the diffractometer control program. Alastair MacDowell developed the manipulator design. During the design and construction stages, the following people worked very hard: Warren Waskiewicz, Laura Norton, Steve Davey, and Jason Stark. In later years the input and contributions of the following people have been invaluable: Ken Evans-Lutterodt, Rolf Schuster, Peter Eng, Peter Bennett, and Don Walko. Finally, the vision and foresight of the Bell-Labs management to finance the whole project, at a time when it was unclear that it would work, deserves great commendation.

LITERATURE CITED

Abernathy, D. 1993. An X-ray Scattering Study of the Si(113) Surface: Structure and Phase Behavior. Ph.D. dissertation, Massachusetts Institute of Technology.

Afanas'ev, A.M. and Melkonyan, M.K. 1983. *Acta Crystallogr. A* 39:207.

Als-Nielsen, J. 1987. Solid and liquid surfaces studied by synchrotron X-ray diffraction. *In* Structure and Dynamics of Surfaces II (W. Schommers and P. von Blanckenhagen, eds.) pp. 181-222. Springer-Verlag, Berlin.

Andrews, S.R. and Cowley, R.A. 1985. *J. Phys. C* 18:6247.

Bloch, J.M. 1985. *J. Appl. Crystallogr.* 18:33.

Born, M. and Wolf, E. 1975. Principles of Optics. Pergamon Press, Elmsford, N.Y.

Busing, W.R. and Levy, H.R. 1967. *Acta Crystallogr.* 22:457.

Coppens, P., Cox, D., Vlieg, E., and Robinson, I.K. 1992. Synchrotron Radiation Crystallography. Academic Press, London.

Dosch, H. 1987. *Phys. Rev. B* 35:2137.

Dosch, H. 1992. Critical Phenomena at Surfaces and Interfaces: Evanescent X-ray and Neutron Scattering. Springer-Verlag, Heidelberg.

Dosch, H., Mailander, L., Reichert, H., Peisl, J., and Johnson, R.L. 1991. *Phys. Rev. B* 43:13172.

Eisenberger, P. and Marra, W.C. 1981. *Phys. Rev. Lett.* 46:1081.

Evans-Lutterodt, K. and Tang, M.T. 1995. Angle calculations for a "2+2" surface X-ray diffractometer. *J. Appl. Crystallogr.* 28:318-326.

Fuoss, P.H. and Robinson, I.K. 1984. Apparatus for X-ray diffraction in ultra-high vacuum. *Nucl. Instr. Methods A* 222:171.

Guinier, A. 1963. X-ray Diffraction. W.H. Freeman, New York.

James, R.W. 1950. The Optical Principles of the Diffraction of X-rays. G. Bell and Sons, London.

Keating, D., Nunes, A., Batterman, B., and Hastings, J. 1971. *Phys. Rev. B* 4:2472.

Keating, P.N. 1966. *Phys. Rev.* 145:637.

Lipson, H. and Cochran, W. 1966. The Determination of Crystal Structures. Cornell University Press, Ithaca, N.Y.

Meyerheim, H.L., Moritz, W., Schulz, H., Eng, P.J., and Robinson, I.K. 1995. Anharmonic thermal vibrations observed by surface X-ray diffraction for Cs/Cu(001). *Surf. Sci.* 333:1422-1429.

Moncton, D.E. and Brown G.S. 1983. *Nucl. Instr. Methods* 208:579.

Müller, B. and Henzler, M. 1995. SPA-RHEED—A novel method in reflection high-energy electron diffraction with extremely high angular and energy resolution. *Rev. Sci. Instrum.* 66:5232-5235.

Parratt, L.G. 1954. *Phys. Rev.* 95:359.

Robinson, I.K. 1986. Crystal truncation rods and surface roughness. *Phys. Rev. B* 33:3830.

Robinson, I.K. 1990a. *Faraday Discuss. R. Soc. Chem.* 89:208.

Robinson, I.K. 1990b. Surface crystallography. *In* Handbook on Synchrotron Radiation, Vol. III (D.E. Moncton and G.S. Brown, eds.) pp. 221-266. Elsevier/North-Holland, Amsterdam.

Robinson, I.K. and Tweet, D.J. 1992. Surface X-ray diffraction. *Rep. Prog. Phys.* 55:599-651.

Robinson, I.K., Eng, P.J., and Schuster, R. 1994. Origin of the surface sensitivity in surface X-ray diffraction. *Acta Phys. Pol. A* 86:513.

Salditt, T., Lott, D., Metzger, T.H., Peisl, J., Vignaud, G., Legrand, J.F., Grübel, G., Høghøi, P., and Schärpf, O. 1996. Characterization of interface roughness in W/Si multilayers by high resolution diffuse X-ray scattering. *Physica B* 221:13-17.

Sheithauer, U., Meyer, G., and Henzler, M. 1986. *Surf. Sci.* 178:441.

Sinha, S.K., Sirota, E.B., Garoff, S., and Stanley, H.B. 1988. X-ray and neutron scattering from rough surfaces. *Phys. Rev. B* 38:2297.

Takayanagi, K., Tanishiro, Y., Takahashi, S., and Takahashi, M. 1985. *Surf. Sci.* 164:367.

Vineyard, G.H.. 1982. *Phys. Rev. B* 26:4146.

Vlieg, E., van der Veen, J.F., Macdonald, J.E., and Miller, M. 1987. Angle calculations for a five-circle diffractometer used for surface X-ray diffraction. *J. Appl. Crystallogr.* 20:330-337.

Warren, B.E. 1969. X-ray Diffraction. Addison-Wesley, Reading, Mass.

Woolfson, M.M. 1997. An Introduction to X-ray Crystallography. Cambridge, Cambridge University Press.

Wormington, M., Bowen, D.K., and Tanner, B.K. 1992. Principles and performance of a PC-based program for simulation of grazing incidence X-ray reflectivity profiles. *Mater. Res. Soc. Symp. Proc.* 238:119-124.

KEY REFERENCES

Als-Nielsen, 1987. See above.

Describes the principls of x-ray reflectivity from an experimental and theoretical point of view.

Dosch, 1992. See above.

Covers the use of evanescent x-ray waves to probe the depth dependence of phase transitions near surfaces.

Robinson, 1990b. See above.

Describes surface structural analysis from a crystallographic perspective.

Sinha et al., 1988. See above.

Describes phenomenological models of surface roughness and derives their signatures in diffraction.

Contributed by I.K. Robinson
University of Illinois
Urbana, Illinois

APPENDIX A: VACUUM PROCEDURE

In order that samples have a chance to remain clean for the duration of an experiment, surface science experiments are usually carried out at pressures of 10^{-10} Torr or below, called the ultrahigh-vacuum (UHV) regime. Under these conditions, according to the kinetic theory of gases, an atom on the surface will be impacted by a residual gas atom from the vacuum about every 30 to 60 min. The vacuum protocols described here apply to the X16A facility at NSLS and are rather specific in this section. At other facilities, the principles will be the same, but the details will be a little different. In the latter case, the information provided here will enable the reader to assess the level of complexity involved in carrying out experiments under UHV.

Load-Lock Procedure

Because preparation of 10^{-10} Torr pressure is time consuming (see below), a load-lock procedure has been developed that allows simple manipulation of samples, thermocouples, and heaters to be carried out without venting the main UHV chamber. The principle of operation is shown in Figure 10d.1.7. Load locking is very useful for batch processing a series of samples, e.g., or for introducing samples that cannot stand to be baked at 150°C.

To load a sample, first ensure that the loading chamber is under vacuum. Its turbopump should have been at full speed for at least 10 min. Then open the gate valve that separates the loading chamber from the main UHV chamber. The pressure may rise into the 10^{-8} Torr range.

Set the diffractometer to the precalibrated angle settings recorded in the logbook or use the preassigned macro definition, called "load." The manipulator is now exactly in line with the sealing surface and can be extended fully until the motor will not move further. As always, when moving the manipulator, it is imperative to watch the progress so as to avoid unexpected collisions. The centering can be verified by observing the final sealing approach through the load-lock window.

Once sealed, the loading chamber is vented with air by (1) depowering the turbopump, (2) isolating the roughing pump (it is not necessary to turn it off), (3) waiting for the pump to slow down significantly (~2 min), and (4) slowly unscrewing its black venting screw while observing the pressure in the main chamber. If the pressure rises, immediately reverse the procedure and reseat the sample.

If the procedure goes well, the UHV conditions of the main chamber will be retained by the electrical and thermal feedthroughs in the design of the manipulator head. The loading chamber can then be unbolted to allow changing of or modification to the sample.

The reverse procedure is to bolt the loading chamber back over the finished sample, open the valve to the roughing pump, and start up the turbopump. Anywhere from 5 to 30 min after the pump reaches full speed, the manipulator can be retracted into the main chamber and the gate valve closed. The pressure may rise momentarily into the 10^{-7}-torr range before dropping to 10^{-10} again. The fresh sample and filaments will now need to be outgassed by heating.

Venting Procedure

When more serious vacuum interventions are required, the entire chamber will need to be vented. The procedure here is similar to that described above, except there are more precautions.

First, turn off all filaments inside the main chamber and disconnect their power cables to avoid accidental activation. The ion gauge is protected and so may be left on. Close the gate valve to the ion pump if this is not to be vented also; otherwise turn off the power here as well.

Manually override the protection circuit to the turbopump gate valve, so that it does not close when the pump is turned off. This is done by powering the solenoid directly. Then the main chamber is vented with nitrogen gas supplied to its vent valve as follows:

1. Depower the turbopump.
2. Isolate the roughing pump (it is not necessary to turn it off).
3. Wait for the pump to slow down significantly (~2 min).
4. Switch on its venting circuit on the turbo control panel.

The pressure has equilibrated with the atmosphere when the bellows become limp. Overpressurization is avoided by a check valve in the nitrogen feed.

Bakeout Procedure

While the main chamber is open, the following routine maintenance may need to be carried out:

1. Replace the sublimation pump filaments.
2. Check the body of the manipulator for shorts or frayed wiring.
3. Recharge evaporation sources.
4. Clean any evaporated deposits from the interior of the windows.

The vacuum restart procedure is the reverse of the venting procedure given above (see Venting Procedure). The next step is the bakeout, which requires considerable disassembly of the diffraction parts of the experiment in order that they do not obstruct the ovens or get unnecessarily hot themselves. The following settings are advised:

1. The variables TTH, TH, CHI, and ALP should be set to zero (270 on dials of TH and TTH). The motor power can now be turned off.
2. The PSD high voltage should be turned off before moving it for storage.
3. Flight path vacuum should be turned off at its Nupro valve. The entire diffractometer TTH arm can now be dismounted and stored.
4. The turbopump gate valve should be in the protect mode (i.e., connected to its controller).

It is necessary to heat all of the chamber walls to 150°C for ~12 hr. This is achieved with ~1000 W of power distributed as follows:

1. Snap together the toggles that hold together the oven walls, which encase the main chamber. Any gaps can be filled with aluminum foil.

2. Lay the heater tape along the length of the manipulator and encase it with its clamshell oven. Any excess tape can be wrapped around the exposed feedthroughs.

3. Place the heater tape around the bellows/seal (between the diffractometer and the chamber).

4. Apply the following power settings: 110 V to each of two oven heaters and one ion pump heater, 60 V to heater tape around chi-bellows/seal; set the manipulator to 110 V if the tape is small (100 W) or to 70 V if the tape is large (300 W).

To shut down the bakeout, it is adequate to follow these quick steps:

1. Turn off all power.

2. About 30 to 60 min later, partially open roof of oven and unwrap the manipulator.

3. Another 30 to 60 min later, finish dismounting the oven.

The expected performance of the pressure will be in the 10^{-7}-torr range at the start, rising to 10^{-6} when hot and eventually dropping to 10^{-7} at the end of the bake. After the heat is turned off, the pressure will fall steadily and reach 10^{-10} Torr in ~12 h.

APPENDIX B: DATA ANALYSIS PROGRAMS

A suite of data analysis programs have been written to perform the various steps of data analysis. The plot program ANA is the most generally useful, while the full set of four programs are needed for a complete surface crystallographic analysis. They were all written by Elias Vlieg and are much more widely used than just at X16A, so their description here will be generally applicable. The programs are designed to work with the data file structure of "super" (Appendix C) but also accept input in other formats, including "spec."

The programs are interactive with the user. The commands to all programs are either keyed in at a prompt or redirected from a macro (*.mac) file. Each entered line is a continuous string of commands and arguments delimited by spaces. The commands are mostly English or Dutch verbs and may be highly abbreviated, usually to a single letter. This is made possible by the use of a hierarchical "menu" structure that defines the logical sequence of allowed commands. Each command is followed immediately by its arguments (separated by spaces) or by a <CR> to be prompted for the arguments. For example, the setup commands specific to plotting in ANA are unreachable at the main level but are reached by typing *p(lot)*. At any level the command *h(elp)* will provide a list of available commands and *l(ist)* will provide current values and status.

Upon exit from any of the programs (except AVE), an executable macro file is generated that records the current options that have been defined during the last session. This file is automatically executed when the program is restarted so that the previous configuration is restored. In the following descriptions the commands are defined by their full names with the minimum abbreviation indicated using the syntax *p(lot)*.

Plot program ANA

This program maintains five data buffers into which spectra can be read. It uses the same buffers for generated fitting curves, so these can be superimposed. A variety of read formats are supported.

The *s(et)* menu is for setting parameters and modes. The *r(ead)* submenu is used to define filenames and column numbers for input. The *f(it)* submenu sets the mode of fitting, e.g., the weighting scheme.

The *r(ead)* menu is for reading in a spectrum and is followed by a format type, a scan number or filename, and a destination buffer number. Example formats are: *s(uper)*, *c(olumn)*, *x(y)*, and *(s)p(ec)*.

The *o(perate)* menu is for manipulating spectra. Mathematical operations are available through the *ad(d)*, *su(m)*, *mu(ltiply)*, and *sh(ift)* commands. Another functions is *l(ump)* for combining adjacent groups of data points within a spectrum. The function *me(rge)* combines two spectra, accounting for monitor counting time and removing duplicate data points; *w(rap)* removes 360° cuts in data; and *d(elete)* removes selected data points while *c(ut)* removes data points above or below a certain specified value.

The *p(lot)* menu makes graphs on the screen that can accumulate multiple entries for later printing or conversion to other image formats. A wide selection of *c(urve)*, *s(ymbol)*, and *li(nestyle)* options are supported. Curves can be *p(lot)*ed fresh or else *o(verlay)*ed and *ax(es)* and *te(xt)* can be supplied and modified. Logarithmic and linear scales can be chosen with, e.g., *ylog* and *xlin*. The program uses a commercial package called "graphi-c" for its plotting functions, and all file conversions of graphical output (including printing) must be handled through its internal mechanisms: hitting the space bar (a few times) allows access to the print menu of "graphi-c", and the simplest printout is activated by *l* for large or *m* for medium size.

The *f(it)* menu performs least-squares fitting to a library of functions. The command is followed by a code for the fit function required, which is assembled from *g(aussian)*, *l(orentzian)*, *v(oigt)*, *p(owerlaw)*, or *k(ummer)* components using commas as delimiters. Finally, the input and output spectrum numbers must be given. For example, the command "f g,l,l 1 2" will fit the sum of a gaussian and two lorentzians to the data in spectrum 1 and put the fit curve in spectrum 2. A two-parameter linear background is always assumed in addition to the chosen functions. Once inside

the fit menu, the options are to *g(uess)* starting values of the parameters, specify a *v(alue)* by hand, and then *f(ix)* or *l(oosen)* these values. Finally, *r(un)* executes the least-squares fit and lists the parameter values.

A useful shortcut is the *a(utoplot)* menu with only two commands, *d(ata)* and *f(it)*. This generates a generic format plot with useful text information superimposed, such as the fitted values of the parameters.

Integration Program PEAK

This is a batch program for converting rscans and jscans (see Appendix C, Important Scan Types) into structure factors. It is assumed that the scans cut directly across the desired diffraction features whose intensity is then related to the square of the structure factor; misalignment will, of course, lead to underestimation of the structure factor. It is also assumed that the scan reaches far enough that the background can be estimated by linear interpolation between its two ends. The "stretching" feature of "super" (see Appendix C, Important Scan Types) is designed to facilitate this.

The program is also responsible for four standard corrections to the data:

1. area correction, due to the changes in the active area of the sample as the diffractometer angles change, introduced by Robinson (1990b);
2. Lorentz factor correction, to convert an angular scan into an integral in reciprocal space, as in Warren (1969);
3. polarization correction, as in James (1950); and
4. monitor and stepsize normalization to account for different counting times and scanning rates that may have been used for different parts of the data.

Under the *c(olumn)* menu, it is necessary that all the diffractometer angles be identified by their column sequence number in the scan file. These must not change from one scan to the next.

The remaining parameters are entered at the command line. The *le(ft)* and *ri(ght)* numbers of points are to be considered as background; all points in between are integrated numerically to a total intensity. The *s(cantype)* can be *r(ocking)* or *i(ndex)* and will affect the Lorentz factor; all other scans found in the batch input will be ignored. For the area correction, the incident beam is taken to have dimensions *wi* vertically by *hi* horizontally, the sample has width *ws*, and the vertical exit beam slit is *we*.

The *r(un)* command followed by starting and ending scan numbers will perform the integration. Two output files are generated. The *.inf file has a line of information about each scan found, such as the date, background, and peak levels. The *.pk file contains the scan number hkl, the structure factor, and the structure factor error as the first three columns.

Averaging Procedure AVE

This procedure uses the *.pk output of PEAK to locate and compare all the symmetry equivalents. It determines an overall estimate of the average systematic error, ε, assumed to be a constant fraction of each individual structure factor value. The value of ε is taken to be a quality factor (R value on structure factors) in assessing the data, as discussed in Robinson (1990b). The program then passes through the data a second time to generate a weighted average value (file *.wgt) of each inequivalent structure factor with an enlarged error bar that combines its statistical errors input with its overall systematic error estimated in the first pass.

The *.ave output listing is very useful for finding bad data. It lists together all reflections that are equivalent according to the specified symmetry. Any that fall out of line are flagged with warnings indicating they should be checked. They are identified by scan number in the listing. This is also a useful way of testing the symmetry of the data, if this is unknown from context, since the program can be run with different preassigned choices of assumed symmetry.

The *s(et)* menu has submenus for defining *c(olumns)*, *s(ymmetry)* from the list of all 17 possible plane groups from p1 to p6mm, and *a(veraging)* parameters and modes. Under *a(veraging)* is the *c(utoff)* parameter, which is the number of times that a structure factor must be larger than its statistical error for it to be used in the estimation of ε. The default value (number of standard deviations) is 2σ, and this should be increased to 10σ if the data are not strongly affected by counting statistics.

Fitting Procedure ROD

This is a large refinement program for fitting a structural model to crystallographic data. It is specific to surface diffraction in that it calculates CTR rather than bulk diffraction structure factors. It differentiates the "bulk" and "surface" parts of the structure and includes a simple description of surface roughness that is usually necessary to get a good fit. The bulk cell is periodic and invariant; it only contributes to the CTRs. The atoms in the surface cell can be selectively refined in position, occupancy, and Debye-Waller factor. It is important that the z coordinates in the surface be a smooth continuation from those of the bulk.

The input files needed for ROD are as follows. All are expected to have a header line that is ignored on input. The second line of the first two files must contain the six unit cell parameters in real space, a, b, and c (in angstroms) and α, β, and γ (in degrees). The program checks that both are the same:

1. bulk unit cell coordinates, *.bul;
2. surface unit cell coordinates, *.sur (fixed), or *.fit (parameterized);
3. structure factor data, *.dat (renamed from *.wgt above); and
4. model parameters, *.par (optional).

In order that small data sets can be compatible with large models, ROD allows a very flexible parameterization scheme. The same displacement, occupancy, and DW parameters can be assigned to more than one atom. This is

very convenient for structures that contain repeated motifs or different symmetries of components within the whole unit cell. In fact, the program does not handle symmetry at all, since this can always be built into the model; all structures are assumed to have triclinic, 1 × 1 unit cells.

APPENDIX C: SUPER COMMAND FORMAT

Commands have a variable number of arguments, depending upon the specific application. Arguments follow on the same line as the command and are separated by spaces or commas. Most commands will prompt the user for the required arguments if no arguments are given. Multiple commands may be placed on one line provided they are separated by a semi-colon.

Values of important control parameters are stored as "variables." To obtain the current value of a variable, type its name followed by =. To change the value stored in a variable, type the new value after the =, e.g., as=1.65. Rudimentary algebra is also allowed, e.g., as=bs * 3. Space characters are required as delimiters around the mathematical operation.

A manual of allowed commands will be available at the beamline. A list of all valid "super" commands can be obtained by typing "help" at the "super" prompt or using the F8 key. Pressing F5 lists the orientation matrix and the values of string variables. The values of all other variables are listed using F6.

Basic Super Commands

mv Move motors (four arguments: TTH, TH, PHI, CHI).

ct Count (one optional argument = preset).

br Go to position defined by *H*, *K*, and *L* (three arguments).

wh Print current *H*, *K*, and *L* and values of the motor angles (no arguments).

ca Calculate motor angles from *H*, *K*, and *L* (three arguments).

ci Calculate *H*, *K*, and *L* from motor angles (five arguments).

end Exit the program.

Basic Super Variables

as Crystal reciprocal lattice parameter a^*

bs Crystal reciprocal lattice parameter b^*

cs Crystal reciprocal lattice parameter c^*

al Crystal reciprocal lattice angle α^*

be Crystal reciprocal lattice angle β^*

ga Crystal reciprocal lattice angle γ^*

wv Incident wave vector ($2\pi/\lambda$)

nobs Number of alignment reflections used to calculate OM

h1, k1, l1, h2, k2, ... HKLs of orientation reflections

t1, u1, p1, c1, a1, u2, p2, ... 2-Theta, theta, phi, chi, and alpha of orientation reflections

B Target value of incidence angle, α_i

B2 Target value of exit angle, α_f

alm Mode of calculating ALP for five-circle geometry (alm=1 means ALP is frozen at its current value; alm=2 means ALP is calculated)

bem Mode of constraining incidence angle for five-circle geometry (bem=1 means *incidence* angle α_i is fixed at target value B; (bem=2 means *exit* angle α_f is fixed at target value B2; bem=3 means incidence and exit angles are made equal)

fchi CHI angle of optical surface orientation (laser alignment)

fphi PHI angle of optical surface orientation (laser alignment)

Orientation Matrix

There are two ways of achieving the sample orientation, depending on whether the reciprocal lattice parameters are known or unknown. In the more commonly used "lattice parameters known" mode, the six reciprocal lattice parameters are entered manually using syntax name = value. The names of the six reciprocal lattice constants are as, bs, cs, al, be, and ga. Two orientation reflections are required with h, k, l, TTH, TH, PHI, CHI, and ALP specified for each reflection. The meaning of the angles is slightly different in different modes of calculating the orientation matrix. We refer here only to the five-circle mode, which is set by the command *frz 5*.

Individual variables in the orientation matrix can be changed using syntax name = value. The variable names in this case consist of a single letter and a number (e.g., t1, t2, t3, ...). The number refers to the number of the orientation reflection. The letters are assigned as follows for the five-circle mode: t = 2-theta, u = theta, p = phi, c = chi, a = alpha, h,k,l = Miller indices, g = gamma (fixed out-of-plane detector position), and z = zeta (fixed sample offset angle).

The orientation reflections may also be entered using the *or* (orient) command. To enter the parameters for the current diffractometer position, type *or* followed by the number of the reflection (in this case 1 or 2) and the hkl. One may also manually enter all variables on one line by typing

or # h k l TTH TH PHI CHI ALP

The orientation matrix is a general 3 × 3 matrix with 9 degrees of freedom described by Busing and Levy (1967). Six degrees of freedom are constrained by the reciprocal lattice parameters, 2 more come from the first orientation reflection (the two polar angles), and the final degree of freedom comes from the second orientation reflection (the second reflection specifies the azimuthal rotation about the

first vector). The direction of the first orientation reflection, called the primary reflection, will always be reproduced exactly. The angles of the second reflection may not necessarily be consistent with the lattice parameters, and consequently the program may not reproduce the angles of the secondary reflection exactly. The *sor n m* command allows reflections n and m to be swapped.

The "lattice parameters unknown" mode is set by toggling the *om* command. Then the six reciprocal lattice parameters are determined directly from the five angles specified for each of the orientation reflections (TTH, TH, PHI, CHI, and ALP). To define the nine matrix elements of the orientation matrix, at least three non-coplanar reflections must be used, so nobs = 3. If nobs3, the best matrix is constructed from the full list of nobs reflections using a least-squares fit and will usually improve as more reflections are added. Reciprocal lattice parameters that are consistent with the three observed reflections will then be calculated. In general, the reciprocal lattice parameters will correspond to a triclinic cell with interfacial angles nearly equal to those expected from the symmetry. As guide to selecting suitable reflections, an error is calculated for each, which is the distance (in reciprocal angstroms) of the reflection from the reciprocal lattice point derived from the orientation matrix. The orientation parameters may be entered manually or by using the *or* command.

Important Scan Types

ascan Angle scan—Scan four diffractometer motors TTH, TH, PHI, CHI.

mscan Motor scan—Scan up to three arbitrary motors.

iscan Index scan—Input three starting HKLs and three delta HKLs for the increments between points.

jscan Centered index scan—Like iscan except scan is *centered* on the given starting hkl value.

kscan Centered two-dimensional index scan—Like jscan it is *centered* on the given starting hkl value. Two sets of delta HKL step sizes are given.

rscan Rocking scan—Input HKL value, motor number (or hkl) and one delta value for the increment. The scan moves either one motor or one hkl component and is centered at the given HKL value.

lup Line-up scan—Input motor number and delta angle. Similar to a rocking scan, but the scan is centered at the current position of the motors. At the end of the scan, the motors move to the peak position, calculated as the center of gravity of the counts measured.

fpk Find peak scan—Like lup, except fewer parameters are required and the data are not saved on disk. After the scan, the motors moved to the peak calculated from the first moment.

vscan Variable scan—Input HKL, variable name, and starting value. The scan increments the value of the variable and moves the motors to the given HKL.

vlup Centered vscan—Input HKL, variable name, delta, and npts. The scan increments the value of the variable and moves the motors to the given HKL. The scan is centered on the current value of the variable beforehand, which is reset to the center of gravity afterward.

pkup Peakup reflection—The scan does a series of lup scans centered at each orientation reflection. At the end of the series, the angles of the orientation reflection are updated to reflect the new peak position.

The scan types *rscan* and *jscan* embody automatic "stretching"' of the background, whereby the step size at the beginning and end of the scan is increased by a factor of 3. The *lup* and *vlup* scans are very useful during the alignment stages of the experiment because of their autocentering feature; they can also be used to make automatic realignments during an unattended batch procedure. All scans generate a video display of the data as they accumulate, which can be viewed at any time using the function keys: F1 (F2) to see the spectrum of the multichannel analyzer as it accumulates and F3 (F4) to see a histogram of the recorded counts on a linear (log) scale.

A scan may be executed by typing the command name followed by a list of arguments. To obtain help on the command format, type the name of the scan without arguments and the program will prompt you. Any scan can be interrupted during execution by ^C and continued by typing *co*. A series of commands (including scans) can be executed by using either the *sc* command or the *ex* command.

To use the *sc* command, one first has to enter a list of commands into the scan table. The list can contain almost any command executable from the command line. A scan list can be created in three ways. The most direct method is to use the *ds* (define scans) command. Alternatively, one can use the *es* (edit scans) command to edit the scan table directly. The command *gs* filename (get scans) will read a new scan table file. Once the scan table has been entered, a list of commands or scans can be executed with the *sc* command, which accepts a series of numbers in arbitrary order corresponding to the position of the command in the scan table. Before execution begins, the program does a "dry run" to check for setting calculation errors and limit problems. If the execution is halted, the *co* command will resume execution.

A series of commands or scans can also be executed with the *ex* command. This command diverts program input to a script file and executes the commands in order. There is no limit to the number of commands in the file. In contrast to *sc*, the *ex* command does not do a dry run before execution begins. If a problem is encountered during execution, the program skips to the next command in the list.